Chemical Geology 622 (2023) 121390

Contents lists available at ScienceDirect

Chemical Geology

journal homepage: www.elsevier.com/locate/chemgeo

Coevolutions of terrestrial temperature and monsoonal precipitation amounts from the latest Pleistocene to the mid-Holocene in Japan: Carbonate clumped isotope record of a stalagmite

Hirokazu Kato [a,*], Taiki Mori [b], Shota Amekawa [a], Chung-Che Wu [c], Chuan-Chou Shen [d,e], Akihiro Kano [a]

[a] Department of Earth and Planetary Science, Graduate School of Science, The University of Tokyo, 7-3-1 Hongo, Tokyo 113-0033, Japan
[b] Chuo Kaihatsu Corporation, 3-13-5 Nishi-Waseda, Shinjuku-ku, Tokyo 169-0051, Japan
[c] Laboratory of Inorganic Chemistry, Department of Chemistry and Applied Biosciences, ETH Zurich, 8093 Zurich, Switzerland
[d] High-Precision Mass Spectrometry and Environment Change Laboratory (HISPEC), Department of Geosciences, National Taiwan University, Taipei 10617, Taiwan, ROC
[e] Research Center for Future Earth, National Taiwan University, Taipei 10617, Taiwan, ROC

ARTICLE INFO

Editor: Christian France-Lanord

Keywords:
Stalagmite
Carbonate clumped isotope
Oxygen isotope
Paleotemperature
Paleoprecipitation
Latest Pleistocene
Holocene
Heinrich stadial
Hypsithermal
East Asian summer/winter monsoons

ABSTRACT

Quantitative paleotemperature reconstruction is a challenging and important issue in paleoenvironmental studies, for which carbonate clumped isotope (Δ_{47}) thermometry is a promising approach. Here we analyzed Δ_{47} values from 66 layers of OT02 stalagmite from Ohtaki Cave in central Japan, covering two separate time intervals (2.6–8.8 and 34.8–63.5 ka) to reconstruct terrestrial temperature and meteoric $\delta^{18}O$ records. The average Δ_{47} temperatures of the Holocene interval and the latest Pleistonece interval were 16.3 °C ± 5.6 °C and 9.7 °C ± 4.6 °C, respectively. The Δ_{47} thermometry also revealed that the cold intervals (5 °C–10 °C) correspond to the Heinrich stadials HSs4–6, and the warm interval (up to 19.9 °C ± 6.0 °C) in middle Holocene (approximately 6–5 ka) accompanied by the Hypsithermal climate optimum. We also reconstructed past meteoric $\delta^{18}O$ by subtracting the temperature effect from stalagmite $\delta^{18}O$. Average meteoric $\delta^{18}O$ was −8.2‰ ± 1.0‰ vs. VSMOW in the Holocene interval and − 8.8‰ ± 0.8‰ in the latest Pleistocene interval. Over centennial timescales, meteoric $\delta^{18}O$ was more negative during colder periods, such as Heinrich stadials and a cooling event around 7 ka, and less negative in warmer periods, such as Hypsithermal warming. A temperature dependency of total ^{18}O fractionation from sea water to precipitation is a likely reason for the negative correlation between temperature and meteoric $\delta^{18}O$. Additionally, East Asian summer monsoon (EASM) brought larger rainfall of less negative $\delta^{18}O$ during the warm periods, whereas larger snow/rainfall of more negative $\delta^{18}O$ brought from East Asian winter monsoon (EAWM) in colder periods. The relative influences from EASM and EAWM were changing in a centennial timescale. $\delta^{18}O$ of OT02 had reflected changes in terrestrial temperature and meteoric $\delta^{18}O$, which are both strongly related to EASM and EAWM.

1. Introduction

The oxygen isotopic composition of stalagmite calcite ($\delta^{18}O_C$) is a key source of information for terrestrial paleoclimates. Nevertheless, paleoclimatic interpretation of stalagmite $\delta^{18}O_C$ should consider two main controlling factors: the temperature of calcite formation and the oxygen isotopic composition of cave drip water ($\delta^{18}O_W$). It is impossible to determine their relative importance by measuring only stalagmite $\delta^{18}O_C$. The classical interpretation used in stalagmite paleoclimatic studies from the East Asian Monsoonal region was that the change in meteoric $\delta^{18}O$ ($\delta^{18}O_{MW}$) is the dominant factor controlling stalagmite $\delta^{18}O_C$ and surpasses other foctors such as temperature change (e.g.,

Abbreviations: East Asian monsoon, EAM; last glacial maximum, LGM; dissolved inorganic carbon, DIC; kinetic isotope effect, KIE; Heinrich stadial, HS; Seto Inland Sea, SIS; East Asian summer monsoon, EASM; East Asian winter monsoons, EAWM; prior calcite precipitation, PCP.

* Corresponding author.
E-mail addresses: h.kato@eps.s.u-tokyo.ac.jp (H. Kato), mori.t@ckc.co.jp (T. Mori), amekawa@eps.s.u-tokyo.ac.jp (S. Amekawa), chwu@ethz.ch (C.-C. Wu), river@ntu.edu.tw (C.-C. Shen), akano@eps.s.u-tokyo.ac.jp (A. Kano).

https://doi.org/10.1016/j.chemgeo.2023.121390
Received 4 July 2022; Received in revised form 9 February 2023; Accepted 13 February 2023
Available online 17 February 2023

Wang et al., 2001). The conventional approach has given a lot of achievements revealing paleoclimatic histories of meteorological conditions, such as monsoon intensities, moisture trajectory, and precipitation seasonality (e.g., Wang et al., 2001; Kato and Yamada, 2016).

However, the effect of meteoric $\delta^{18}O_{MW}$ is not always dominant in the stalagmite records. The importance of temperature signals was reaffirmed for late Pleistocene to middle Holocene stalagmites from Mie and Gifu Prefectures, central Japan, located at the eastern margin of the East Asian monsoon (EAM) regime (Mori et al., 2018; Fig. 1). These stalagmites exhibit notably smaller amplitudes of variation in $\delta^{18}O_C$ less than half of Chinese cave records of relevant age; hence, the glacial/interglacial contrast within these stalagmites can be accounted for a typical warming temperature of 9 °C from the last glacial maximum (LGM) to the mid-Holocene (Mori et al., 2018). This estimated temperature change is comparable with other paleoclimate studies using stalagmites and lake and marine deposits around the Japanese Islands (Nakagawa et al., 2002; Kawahata et al., 2011; Kigoshi et al., 2014; Uemura et al., 2016). Mori et al. (2018) concluded that climate effect on $\delta^{18}O_W$ values was insignificant for these Japanese caves, perhaps because of their proximity to moisture sources in the Pacific.

Temperature and precipitation often covary spatially and temporally (discussed in datail later), and signals from these two factors are difficult to be separated in paleoclimatic records. To reconstruct their coevolution, their signals should be divided quantitatively. Recently, it became possible to separate the signals of temperature change in stalagmite $\delta^{18}O_C$ by virtue of advances in various methods to analyze inclusions in stalagmite, i.e., water inclusion and organic contaminants (TEX86 thermometer; e.g., Wassenburg et al., 2021). Another independent approach to estimate paleotemperature is carbonate clumped isotope (Δ_{47}) thermometry (Ghosh et al., 2006; Eiler, 2007). The method has an advantage in its availability because the target substance of the method is carbonate which is the main component of stalagmite. The principle of clumped isotope thermometry is based on the temperature dependency of the observed abundance anomaly of the $^{13}C—^{18}O$ bond in carbonate relative to the stochastic abundance calculated using bulk $\delta^{13}C$ and $\delta^{18}O$ values. The abundance anomaly of $^{13}C^{18}O^{16}O$ (Δ_{47}) in CO_2 from acid digestion of carbonate minerals is negatively correlated with the temperature of carbonate precipitation (Ghosh et al., 2006; Schauble et al., 2006). Nevertheless, estimating paleotemperature from stalagmite Δ_{47} values is challenging. CO_2 degassing from cave water leads to isotopic disequilibrium in the dissolved inorganic carbon (DIC) pool and thus a lower Δ_{47} value of carbonate, which yields higher temperatures than predicted (e.g., Guo and Zhou, 2019). A first step of CO_2 degassing is caused by physical diffusion from cave water to cave atmosphere, and the solution becomes supersaturated with respect to calcite. During calcite precipitation, CO_2 is generated and escapes from the solution. A recent study indicated this precipitation driven degassing solely causes isotopic disequilibrium in DIC (Dreybrodt and Fohlmeister, 2022). The kinetic isotope effects (KIEs) under these conditions have been reported from natural and laboratory speleothem Δ_{47} results (Affek et al., 2008, 2014; Daëron et al., 2011; Kluge and Affek, 2012; Affek, 2013; Affek and Zaarur, 2014; Kato et al., 2021). In our previous study (Kato et al., 2019), we analyzed Δ_{47} values of Japanese natural tufa. Similar to stalagmite settings, CO_2 degassing induces calcite precipitation in tufa by increasing its saturation state in stream water (Ford and Pedley, 1996; Kano et al., 2003, 2019; Kawai et al., 2006).

In another previous study of us (Kato et al., 2021), we measured Δ_{47} values of a stalagmite Hiro-1 from Maboroshi Cave in Hiroshima Prefecture, southwestern Japan (Shen et al., 2010; Hori et al., 2013, 2014; Fig. 1). We applied the temperature calibration evaluated from Δ_{47}

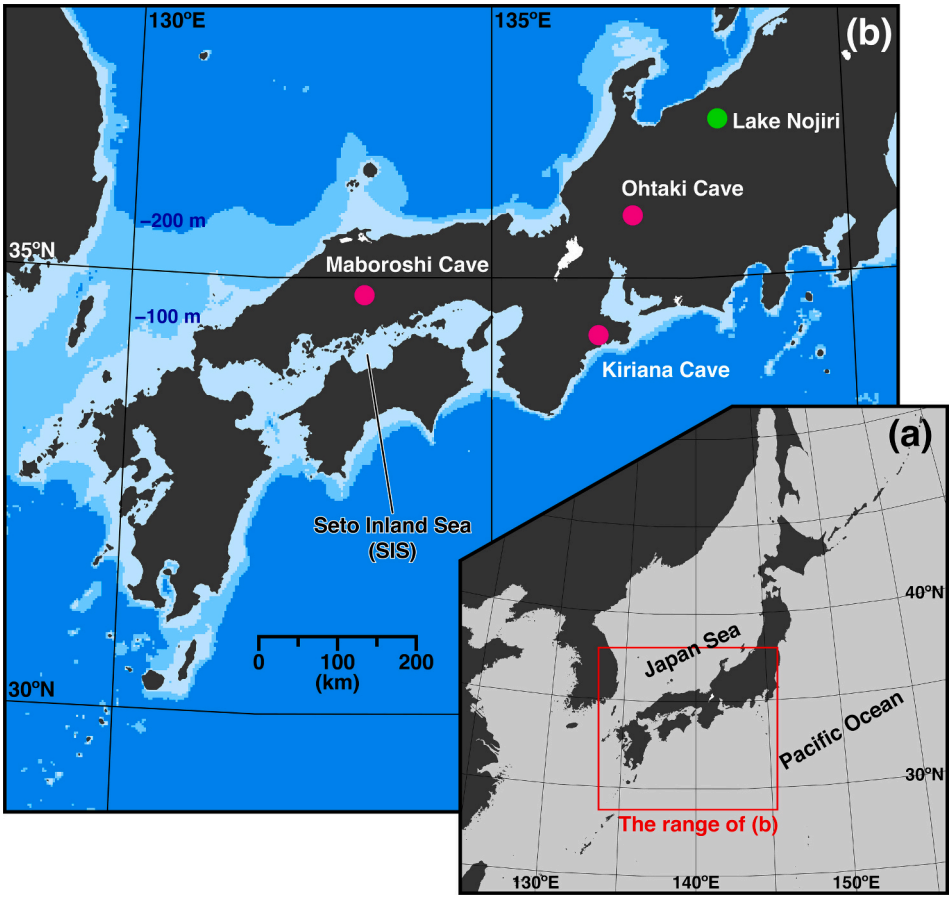

Fig. 1. Maps of study sites. (a) Location of our study area and (b) bathymetric map of western Japan showing the locations of Ohtaki Cave, Maboroshi Cave, Kiriana Cave, and Lake Nojiri.

values of tufa (Kato et al., 2019) to the Δ_{47} values of Hiro-1 stalagmite and revealed terrestrial temperature changes after the LGM to the mid-Holocene, except for some layers in which Δ_{47} and $\delta^{18}O_C$ were significantly disturbed by strong KIE. The Δ_{47} values of Hiro-1 exhibit an abrupt warming which corresponds to the Hypsithermal event (Wanner et al., 2008), but the record during the corresponding Heinrich stadial 1 (HS1) was unavailable because of strong influences of KIE related to dry cave conditions (Kato et al., 2021).

In this study, we analyzed the Δ_{47} values of the OT02 stalagmite (2.6–8.8 and 34.8–63.5 ka; Mori et al., 2018) from Ohtaki Cave (Fig. 1) to obtain a longer climatic record in Japan, including four periods of Heinrich stadials (HSs) that have yet to be clarified in Japan. Mori et al. (2018) recognized the four times of positive excursions of $\delta^{18}O_{OT02}$ as Heinrich stadials (HSs4–6 including 5.2) by comparing with $\delta^{18}O$ curves of Greenland ice core (NGRIP Members, 2004) and that of another stalagmite (KA03 from Kiriana Cave; Mori et al., 2018).

Ohtaki Cave is located 250 km east-northeast from Maboroshi Cave (Fig. 1). The climatic and hydrological settings are different in the Ohtaki and Maboroshi Caves (Kato et al., 2021), although these regions are on the mainland (Honshu) of Japan (Fig. 1). A major difference between the climatic settings of these caves is the seasonal bias in precipitation amount. The averaged winter rain/snowfall in the Ohtaki Cave region is over 500 mm, which is nearly four times of that in the Maboroshi Cave region. In addition, Ohtaki Cave lies 200 km far from the Seto Inland Sea (SIS), which is presumed to be an important source of moisture for the Maboroshi Cave (Fig. 1; Kato et al., 2021). Detailed and statistic comparison of climatic settings of these two cave regions will be performed in a discussion part (Section 5.1). We compare the coevolutions of terrestrial temperature and precipitation in the Ohtaki Cave region from the latest Pleistocene to the middle Holocene, with results from the Hiro-1 stalagmite (Kato et al., 2021) and other studies that revealed EAM evolutions, such as the record from a Japanese lake (Nakamura et al., 2013) and records from Chinese continental regions where many EAM studies have been reported (Porter and An, 1995, 1700 km WSW from our study area; Wang et al., 2001, 2500 km W; Song et al., 2018, 1900 km WNW).

2. Study area and material

2.1. Ohtaki Cave

Ohtaki Cave (35°44′N, 136°59′E; 400 m asl at the entrance) is located in central Gifu Prefecture, Honshu, 80 km away from both the Pacific and Japan Sea coasts (Fig. 1). The region lies on the west of Hida, Kiso Akaisi montain ranges which bisect Honshu. As measured at Nagataki (altitude: 430 m asl; 25 km NNW from the cave), a nearby meteorological station, the annual average rainfall over the latest 40 years was 3081 mm. The region is wet year-round: 22.6% in spring (March–May), 36.0% in summer (June–August), 24.6% in autumn (September–November), and 16.8% in winter (December–February). The 40-year mean annual average temperature is 11.5 °C, ranging from −0.3 °C in January to 23.9 °C in August (Fig. 2a).

Ohtaki Cave has a total length of >1000 m (Yura, 2011) into the Permian limestone of the Mino Terrane (Kajita et al., 1971). It comprises

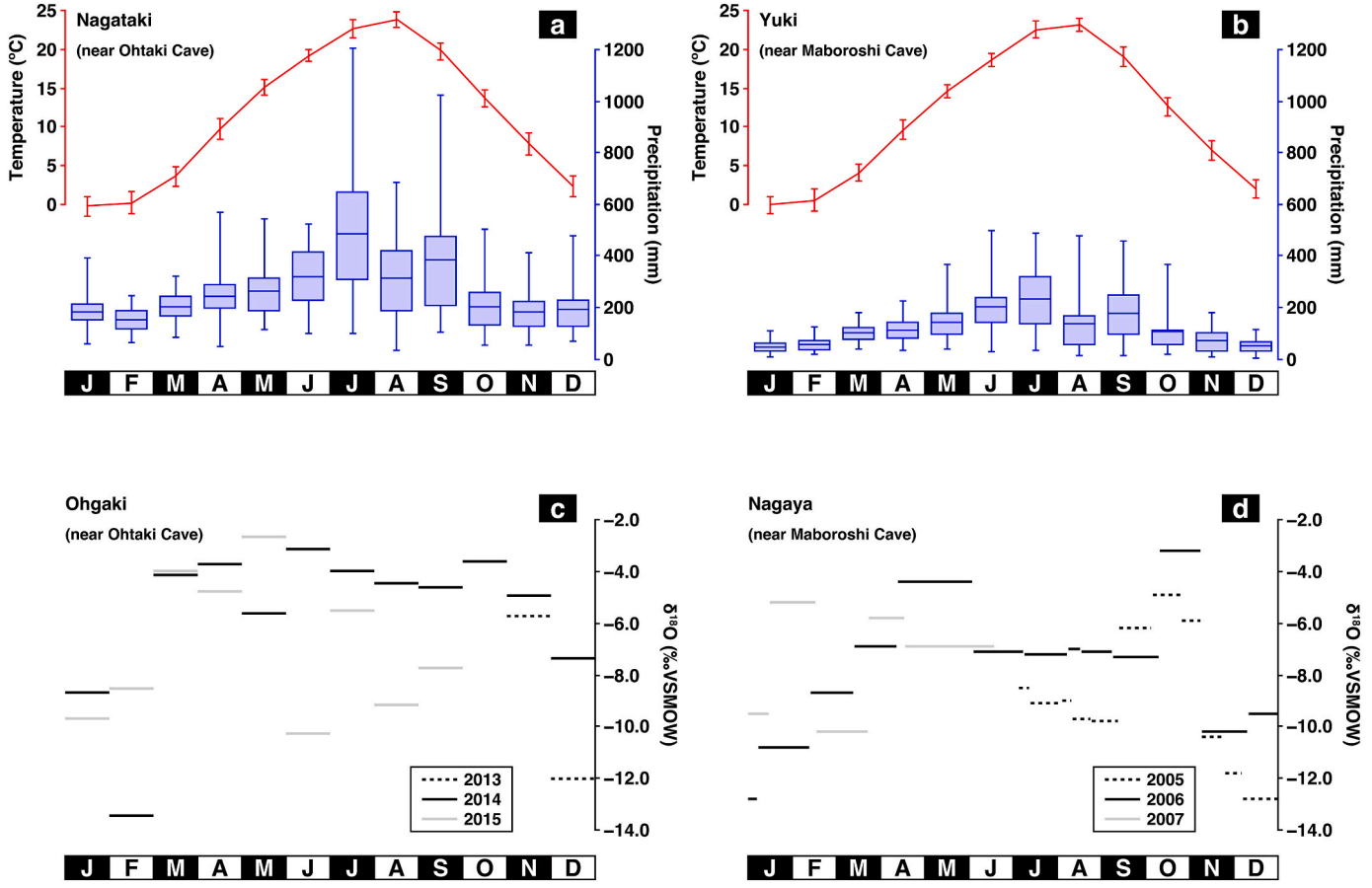

Fig. 2. Climatic conditions at the (a) Nagataki and (b) Yuki observatories over the period 1981–2020 and the oxygen isotopic compositions of meteoric water at (c) Ohgaki and (d) Nagaya. (a, b) Average monthly air temperatures are shown with errors of 1σ. The box plot of precipitation shows the first and third quartiles, and the whisker lengths depict the ranges between the minimum and maximum values. Averaged monthly precipitation is shown by horizontal bars in the boxes. (c, d) Rainwater was collected for each rain event at Ohgaki city, 60 km southwest from Ohtaki Cave, by Mori et al. (2018) and for each month at Nagaya, 20 km east from Maboroshi Cave, by Hori et al. (2009). The bars in (c) show the weighted average values for each month.

three cave levels; stalagmites are best developed in the middle level, which is located 110 m underground. The cave has been modified by artificial tunnels for tourists, but the temperature in the cave remains stable at approximately 13.0 °C, which is not sensitive to the seasonal change in surface temperature but higher than the annual mean temperature observed in the nearest weather observatory at Nagataki (11.5 °C). A larger amount of water seepage during summer possibly elevates the cave water temperature throughout the year.

2.2. Material

We analyzed a 140-mm-long stalagmite (OT02) collected from the middle level, 200 m from the cave entrance. U-Th ages and $\delta^{18}O$ values from OT02 have been reported by Mori et al. (2018). The age model of OT02 was established on the basis of U-Th ages from 11 horizons using a Bayesian statistical model (StalAge; Scholz and Hoffmann, 2011). A hiatus of 26 kyr (8.8–34.8 ka) was recognized at a discontinuous surface at the 55 mm horizon (Mori et al., 2018). The age ranges of the upper and lower parts are 2.6–8.8 and 34.8–63.5 ka, respectively; however, the linear age model of OT02 established by the Bayesian statistical model includes a relatively large uncertainty (up to ±2.5 kyr; Mori et al., 2018). The lower part of OT02 stalagmite records four Heinrich stadials (HSs4–6 including HS5.2). OT02 passed Hendy test (Hendy, 1971) performed for eight depths of the stalagmite to evaluate kinetic effects (Mori et al., 2018).

The $\delta^{18}O_{OT02}$ (VPDB) values range from −8.2‰ to −6.3‰, which were analyzed from 644 layers (at 0.2 mm intervals) of the stalagmite (Fig. 3a; Mori et al., 2018). At 63.5–34.8 ka, the $\delta^{18}O_{OT02}$ generally becomes less negative from older to younger layers and displays four millennial-scale events with amplitude of 0.5‰–1‰. The $\delta^{18}O_{OT02}$ values of the Holocene interval (8.8–2.6 ka) mostly fall between −7‰ and − 8‰; however, a slight positive shift of about 0.5‰ is observed around 6 ka (Fig. 3a). Mori et al. (2018) suggested that the overall trend of $\delta^{18}O_{OT02}$, with a broad positive shift in 63.5–34.8 ka and more negative values in the Holocene, is the same as that of seawater $\delta^{18}O$ (Fig. 3b). The positive excursions of $\delta^{18}O_{OT02}$ corresponding to four Heinrich stadials were observed in the U-Th ages of OT02 at −61.8 ka (HS6), 56.3–55.1 ka (HS5.2), 48.2–44.9 ka (HS5), and 40.9–38.2 ka (HS4). Mori et al. (2018) linked these four durations with terms of HSs found in a KA03 stalagmite (63.5–60.1 ka, 55.9–54.7 ka, 49.4–48.2 ka, and 41.3–39.7 ka), for which the U-Th age model is more precise than the OT02 age model. The similarity of the two stalagmite records also constitutes a "replication test" (Dorale and Liu, 2009), verifying the lack of strong kinetic effects in these records.

2.3. Climatic and hydrological settings of Ohtaki and Maboroshi Caves

Two major moisture sources to Japan are the Pacific Ocean and the

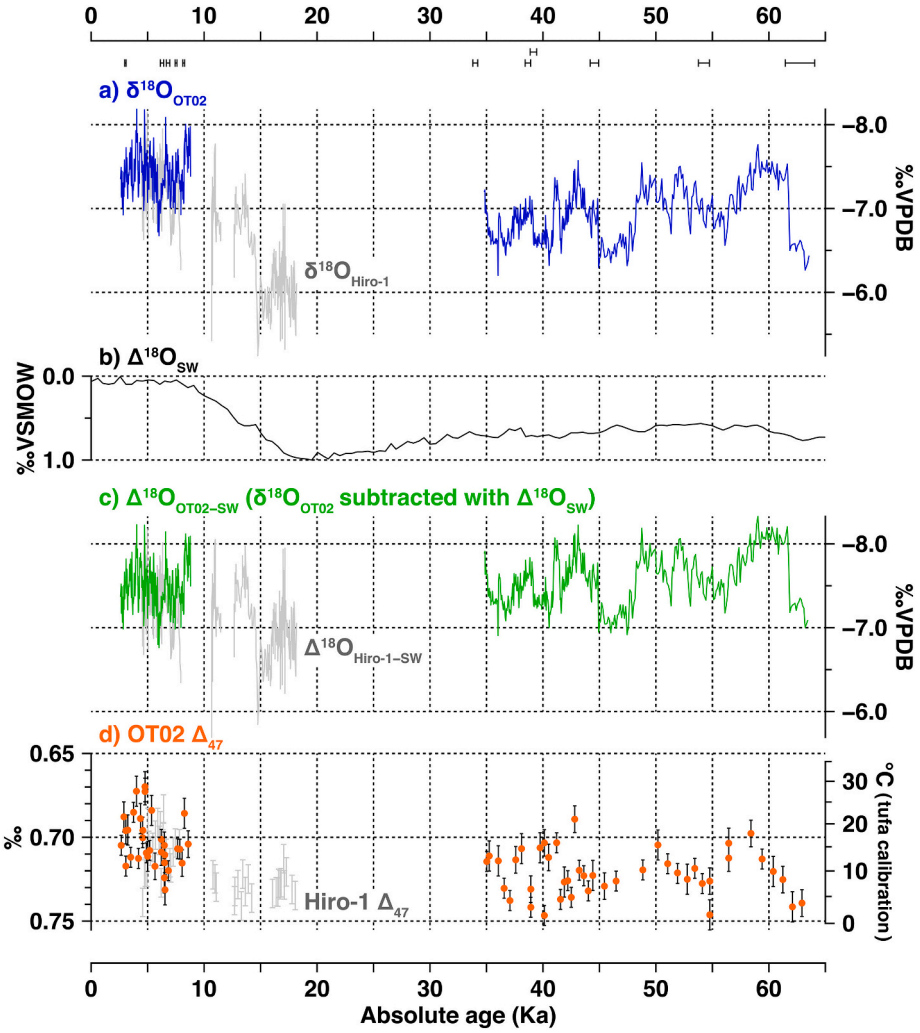

Fig. 3. (a) Time series changes of $\delta^{18}O_{OT02}$ (Mori et al., 2018), (b) $\delta^{18}O_{SW}$ (modified from Lisiecki and Stern, 2016), (c) $\Delta^{18}O_{OT02-SW}$, and (d) Δ_{47} of OT02. The error bars of Δ_{47} show the SD of in-house standard measurements (±‰). Data for OT02 (a, c, and d) are shown alongside (a) $\delta^{18}O_{Hiro-1}$, (c) $\Delta^{18}O_{Hiro-1-SW}$, and Δ_{47} of Hiro-1 (Hori et al., 2013; Kato et al., 2021) as gray lines and bars.

Japan Sea, from which the East Asian summer and winter monsoons (EASM and EAWM, respectively) bring moisture mainly by warm southerly winds and cold northerly winds, respectively. The climate of Japan is characterized by clear seasonality because the East Asian summer/winter monsoons migrate across the region. Consequently, the precipitation source switches seasonally between the Pacific Ocean in summer and the Japan Sea in winter (Fukui, 1977). On the Pacific side of the central mountains in Japan, including the sites of Ohtaki Cave (OT02) and Maboroshi Cave (Hiro-1), the EASM delivers the majority of the annual precipitation to the Pacific side of Japan. During the winter, the cold and dry EAWM winds acquire moisture from the Tsushima Warm Current, which blows into the Japan Sea. Most moisture from the Japan Sea side is then released as heavy snow and rainfall on the Japan Sea coast, whereas residual moisture generates comparatively short snow and rainfall on the Pacific side. Consequently, less negative $\delta^{18}O_{MW}$ values are observed during the warm season, and more negative $\delta^{18}O_{MW}$ values are observed during the cold season in several areas in Japan.

Mori et al. (2018) collected 13 samples of cave drip water at stalagmite OT02, as well as 137 separate rain events in 2013–2015 at Ohgaki City (altitude 10 m), located 60 km southwest from upstream along the major moist trajectory during the EASM season. The $\delta^{18}O_{MW}$ values at Ohgaki show clearer seasonal differences, i.e., less negative values from March to November (−5.7‰ ± 2.3‰ in amount-weighted average) and more negative values from December to February (−10.8‰ ± 2.1‰; Mori et al., 2018; Fig. 2c). The cave drip water likely has $\delta^{18}O$ value near the weighted average of $\delta^{18}O_{MW}$ at Ohtaki Cave, because the region is wet year-round as mentioned above. However, the drip water $\delta^{18}O$ value at Ohtaki (−8.3‰ on average) is clearly more negative than the average $\delta^{18}O_{MW}$ value at Ohgaki (−6.4‰; Mori et al., 2018). This discrepancy is explained by locations along the dominant path of moisture trajectory and differences in altitude; Ohtaki Cave is further from the Pacific and at a higher altitude (400 m asl) than Ohgaki (10 m asl). Previous studies of the meteoric water $\delta^{18}O$ in the Japanese Islands also indicates that the value in the Ohtaki area is clearly more negative than the Ohgaki area (Mizota and Kusakabe, 1994). Asai et al. (2014) investigated monthly $\delta^{18}O_{MW}$ values at 11 locations on Mt. Ontake (1030–2750 m asl), 45 km east–northeast of Ohtaki Cave, in 2003–2005. The $\delta^{18}O_{MW}$ values in the region were least negative in spring (April–May; approximately −10‰ to −8‰), most negative in winter (January–February; approximately −15‰ to −14‰), and moderate during the summer (Asai et al., 2014). Although the altitudes of these sites (Nagaya, Ohgaki, and Ontake) differ significantly from that of Ohtaki Cave, there is a common trend in that the most negative $\delta^{18}O_{MW}$ values were observed in winter. Since Ohgaki is located upstream of Ohtaki along the major moisture trajectory of the region, the seasonal pattern of $\delta^{18}O_{MW}$ around Ohtaki Cave is likely most similar to that in Ohgaki, although the average $\delta^{18}O_{MW}$ is more negative in Ohtaki.

Hori et al. (2009) collected meteoric water at monthly intervals at Nagaya (Okayama Prefecture), located 20 km east of the site of Hiro-1 in 2005–2007. $\delta^{18}O_{MW}$ exhibited less negative values from April to October (−7.1‰ ± 1.4‰ in amount-weighted average) and more negative values from November to March (−9.7‰ ± 1.4‰; Hori et al., 2009; Fig. 2d).

3. Method

3.1. Carbonate clumped isotope (Δ_{47})

3.1.1. Δ_{47}measurement and calculation

We collected subsamples for carbonate clumped isotope (Δ_{47}) measurement from 66 layers throughout OT02. To avoid strong disequilibrium effects as much as possible, subsamples were collected from clear layers excluding opaque and muddy horizons. Such horizons are presumed to have formed under depressed and/or discontinuous calcite precipitation which may be involved to high prior calcite precipitation (PCP) condition and strong disequilibrium imprints (Kato et al., 2021).

Five milligrams of powdered carbonate were digested by phosphoric acid at 90 °C for ~5 min and the generated gas was immediately trapped by a stainless-steel tube cooled by liquid nitrogen. Moisture was separated from CO_2 gas using a liquid nitrogen and ethanol slush, after which CO_2 was introduced to a 30-m-long capillary column (Supel-Q PLOT) with a helium carrier gas. The column was cooled to −10 °C to remove organic contaminants. Purified CO_2 was analyzed with a dual inlet mass spectrometer (Finnigan MAT-253) at Kyushu University configured for measurements of masses 44–49 with pressure adjustment to produce an m/z 44 signal of 16 V. The integration time was 30 s. We applied the Pressure Baseline correction of He et al. (2012) with the off-peak measurement of the background intensities of masses 45–49. Each analysis comprised 5–8 acquisitions, with 4.5 off-peak (nine alternate detections; five times for the reference side and four times for the sample side), 8 on-peak, and 4 off-peak cycles per acquisition.

Further data processing to obtain Δ_{47} values was performed using Microsoft Excel spreadsheets that first provided Δ_{47} value versus working gas (Oztech; $\delta^{13}C$ = −3.61‰ VPDB, and $\delta^{18}O$ = 24.90‰ VSMOW). We applied the ^{17}O correction of Brand et al. (2010) (with K = 0.01022461, λ = 0.528) to calculate Δ_{47} values. Each Δ_{47} value was adjusted on the absolute reference frame of Dennis et al. (2011) and expressed as $\Delta_{47\text{-ARF}}$. Raw $\Delta_{47\text{-[EGvsWG]}}$ was 1) corrected using the δ^{47}-dependence slope (−0.000064‰ in Δ_{47} per 1‰ of δ^{47}; Kato et al., 2019), 2) converted to $\Delta_{47\text{-RF}}$ using an empirical transfer function, and 3) converted to $\Delta_{47\text{-ARF}}$ by adding the acid fractionation factor (0.082‰) of Defliese et al. (2015). We describe $\Delta_{47\text{-ARF}}$ simply as Δ_{47} unless otherwise noted.

Δ_{47} measurements were performed for four discrete periods from 2018 to 2019. Each subsample was measured once or twice, and repeated measurements of an in-house calcite standard (Hiroshima standard; $\delta^{13}C = -0.47‰$, $\delta^{18}O = -5.04‰$ and $\Delta_{47} = 0.671‰$) for 11, 5, 7, and 6 times for each period demonstrated the stability of Δ_{47} measurements. The standard deviations (1 SD) of Δ_{47} measurements were calculated for each period and were found to be ±0.006‰–0.009‰ (n = 5–11), corresponding to ±1.8 °C–3.7 °C in the OT02 temperature range (Table 1).

3.1.2. Temperature calibration for stalagmite Δ_{47}value

To estimate paleotemperature from Δ_{47} values of OT02 stalagmite, we applied an experimental (empirical) calibration established from Δ_{47} values of natural tufa (Eq. (1); Kato et al., 2019).

$$\Delta_{47} = (0.0336 \pm 0.0036) \times 10^6/T^2 + (0.301 \pm 0.048) \quad (1)$$

where T is absolute temperatures in Kelvins. The Δ_{47} temperature calibration of tufa (Eq. (1)) was applied to the Δ_{47} values of Hiro-1 stalagmite and successfully yielded the paleotemperature; average temperature of the middle Holocene part brackets the modern average air temperature, and the Δ_{47} temperature record from Hiro-1 is consistent with well-known climatic stages (Kato et al., 2021). Affek and Zaarur (2014) reported a temperature calibration established from Δ_{47} of $CaCO_3$ rafts floating at the surface of the $Ca(HCO_3)_2$ solutions. The calibration was reculcurated with the ^{17}O correction of Brand et al. (2010) by Matthews et al. (2021) and may be relevant to speleothem conditons. We append a calculation results with the raft calibration in a supplementary file (Table S2).

3.2. Paleometeoric $\delta^{18}O$ reconstruction

As mentioned above, stalagmite $\delta^{18}O_C$ value is controlled by the temperature of calcite formation and the $\delta^{18}O_W$ value of water. Using the paleotemperature determined by carbonate clumped isotope and the temperature dependency of isotopic fractionation between calcite and water ($FT_{water–stalagmite}$), past $\delta^{18}O_W$ values can be calculated from the calcite $\delta^{18}O_C$ value. We applied the temperature dependency of $\delta^{18}O$ of

Table 1
$\delta^{18}O_{OT02}$ and Δ_{47} values of OT02, $\Delta^{18}O_{OT02-SW}$, Δ_{47} temperatures calculated from a tufa calibration (Kato et al., 2019), and reconstructed meteoric water $\delta^{18}O_{MW}$ and $\Delta^{18}O_{MW-SW}$ values.

Analysis	Depth	Age	$\delta^{18}O_{OT02}$	$\Delta^{18}O_{OT02-SW}$	$\Delta_{47\text{-ARF}}$			Δ_{47} temperature			$\delta^{18}O_{MW}$			$\Delta^{18}O_{MW-SW}$		
Number	(mm)	before A.D.	(‰ VPDB)	(‰ VPDB)	(‰)		SE	(°C)	Max	Min	(‰ VSMOW)	Max	Min	(‰ VSMOW)	Max	Min
633	0.5	2663	−7.2	−7.2	0.705	±	0.006	15.3	17.4	13.2	−8.0	−7.6	−8.4	−8.0	−7.6	−8.4
535	2.5	2897	−7.3	−7.4	0.688	±	0.009	21.5	25.0	18.2	−6.9	−6.2	−7.5	−6.9	−6.3	−7.6
618	4.0	3071	−7.3	−7.4	0.717	±	0.006	11.0	13.0	9.0	−8.9	−8.5	−9.3	−9.0	−8.6	−9.4
756	4.0	3071	−7.4	−7.5	0.696	±	0.008	18.5	21.4	15.6	−7.6	−7.0	−8.1	−7.7	−7.1	−8.2
557	5.5	3246	−7.5	−7.6	0.696	±	0.009	18.6	22.0	15.3	−7.6	−7.0	−8.3	−7.7	−7.1	−8.4
684	7.0	3501	−7.5	−7.6	0.712	±	0.006	12.8	14.9	10.7	−8.7	−8.3	−9.1	−8.8	−8.4	−9.2
647	10.5	3756	−7.4	−7.4	0.685	±	0.006	22.6	24.9	20.3	−6.8	−6.4	−7.2	−6.8	−6.4	−7.3
544	12.0	4011	−8.2	−8.2	0.673	±	0.009	27.5	31.2	24.0	−6.7	−6.0	−7.3	−6.7	−6.1	−7.4
703	13.5	4187	−7.6	−7.6	0.713	±	0.006	12.5	14.6	10.5	−8.9	−8.5	−9.3	−8.9	−8.5	−9.3
553	15.0	4363	−7.8	−7.8	0.689	±	0.009	21.1	24.6	17.8	−7.5	−6.8	−8.1	−7.5	−6.9	−8.1
634	16.5	4567	−7.8	−7.8	0.700	±	0.006	16.9	19.1	14.8	−8.2	−7.8	−8.6	−8.3	−7.9	−8.7
870	16.5	4567	−7.9	−7.9	0.696	±	0.008	18.5	21.5	15.7	−8.0	−7.5	−8.6	−8.1	−7.5	−8.6
539	18.5	4771	−7.8	−7.9	0.670	±	0.009	28.6	32.4	25.0	−6.2	−5.5	−6.8	−6.2	−5.6	−6.9
765	18.5	4771	−7.9	−7.9	0.673	±	0.008	27.5	30.7	24.3	−6.4	−5.8	−7.0	−6.4	−5.9	−7.0
695	19.5	4888	−8.0	−8.0	0.709	±	0.006	13.7	15.8	11.6	−9.1	−8.7	−9.5	−9.1	−8.7	−9.5
562	20.5	5006	−8.1	−8.1	0.711	±	0.009	13.0	16.1	9.9	−9.3	−8.7	−9.9	−9.4	−8.7	−10.0
671	22.0	5182	−7.9	−7.9	0.708	±	0.006	14.2	16.3	12.1	−8.9	−8.5	−9.3	−8.9	−8.5	−9.3
548	23.5	5358	−8.1	−8.1	0.684	±	0.009	23.0	26.5	19.6	−7.4	−6.8	−8.1	−7.5	−6.8	−8.1
731	26.0	5655	−7.9	−8.0	0.717	±	0.008	10.9	13.7	8.3	−9.5	−9.0	−10.1	−9.6	−9.0	−10.1
620	31.0	6217	−7.6	−7.6	0.701	±	0.006	16.6	18.7	14.4	−8.1	−7.7	−8.5	−8.2	−7.8	−8.6
758	31.0	6217	−7.5	−7.6	0.709	±	0.008	13.1	16.7	11.1	−8.7	−8.0	−9.1	−8.7	−8.1	−9.1
559	33.0	6483	−7.5	−7.6	0.724	±	0.009	8.6	11.6	5.7	−9.6	−9.0	−10.2	−9.7	−9.1	−10.3
865	33.0	6483	−7.6	−7.7	0.705	±	0.008	15.3	18.1	12.5	−8.4	−7.8	−8.9	−8.4	−7.9	−9.0
685	34.0	6502	−7.6	−7.7	0.715	±	0.006	11.6	13.7	9.6	−9.1	−8.7	−9.5	−9.1	−8.7	−9.5
663	35.5	6522	−7.7	−7.7	0.711	±	0.006	13.3	15.4	11.2	−8.8	−8.4	−9.2	−8.9	−8.5	−9.3
546	36.5	6541	−7.4	−7.5	0.731	±	0.009	6.3	9.2	3.4	−10.0	−9.4	−10.6	−10.1	−9.5	−10.7
708	38.0	6843	−7.4	−7.4	0.720	±	0.006	10.0	12.1	8.1	−9.2	−8.8	−9.6	−9.2	−8.8	−9.6
696	43.5	7650	−7.3	−7.4	0.707	±	0.006	14.6	16.7	12.5	−8.3	−7.8	−8.7	−8.3	−7.9	−8.7
672	45.5	7853	−7.3	−7.4	0.707	±	0.006	14.5	16.6	12.4	−8.2	−7.8	−8.6	−8.3	−7.9	−8.7
732	47.5	8056	−7.4	−7.5	0.715	±	0.008	11.6	14.3	8.9	−8.9	−8.3	−9.4	−9.0	−8.4	−9.5
542	49.0	8259	−7.5	−7.6	0.686	±	0.009	22.3	25.8	19.0	−6.9	−6.3	−7.5	−7.0	−6.4	−7.6
759	52.0	8595	−7.5	−7.6	0.704	±	0.008	15.5	18.4	12.7	−8.2	−7.7	−8.7	−8.3	−7.8	−8.9
689	55.0	35,024	−7.0	−7.7	0.714	±	0.006	11.9	14.0	9.9	−8.4	−8.0	−8.8	−9.1	−8.7	−9.5
564	56.0	35,243	−6.7	−7.4	0.711	±	0.009	13.0	16.2	10.0	−7.9	−7.3	−8.5	−8.6	−8.0	−9.2
550	59.5	36,046	−7.0	−7.7	0.714	±	0.009	12.0	15.2	9.0	−8.4	−7.8	−9.0	−9.1	−8.5	−9.7
664	61.5	36,560	−6.5	−7.2	0.730	±	0.006	6.6	8.5	4.6	−9.0	−8.6	−9.4	−9.7	−9.3	−10.1
709	64.0	37,074	−6.5	−7.1	0.738	±	0.006	4.2	6.1	2.3	−9.5	−9.1	−9.8	−10.1	−9.7	−10.5
761	67.0	37,587	−6.7	−7.3	0.713	±	0.008	12.2	15.0	9.5	−8.1	−7.5	−8.6	−8.7	−8.1	−9.2
536	68.0	38,101	−6.9	−7.5	0.707	±	0.009	14.6	17.8	11.4	−7.8	−7.2	−8.4	−8.4	−7.8	−9.0
697	71.0	38,924	−6.9	−7.6	0.742	±	0.006	2.9	4.8	1.1	−10.2	−9.8	−10.6	−10.9	−10.5	−11.3
762	71.0	38,924	−7.0	−7.7	0.731	±	0.008	6.4	9.0	3.8	−9.5	−9.0	−10.1	−10.2	−9.7	−10.8
558	75.0	39,747	−6.8	−7.5	0.706	±	0.009	14.8	18.0	11.6	−7.7	−7.1	−8.3	−8.4	−7.8	−9.0
676	76.5	40,122	−6.8	−7.5	0.747	±	0.006	1.4	3.3	−0.4	−10.3	−10.0	−10.7	−11.0	−10.6	−11.4
860	76.5	40,122	−6.7	−7.4	0.703	±	0.008	15.8	18.7	13.0	−7.4	−6.8	−7.9	−8.1	−7.5	−8.6
733	78.5	40,498	−6.7	−7.4	0.712	±	0.008	12.7	15.5	10.0	−8.0	−7.4	−8.5	−8.7	−8.1	−9.2
626	81.5	41,212	−7.0	−7.7	0.703	±	0.006	15.8	18.0	13.7	−7.6	−7.2	−8.0	−8.3	−7.9	−8.7
690	83.0	41,551	−6.6	−7.3	0.737	±	0.006	4.4	6.3	2.6	−9.5	−9.1	−9.9	−10.2	−9.8	−10.6
554	84.0	41,890	−6.9	−7.6	0.727	±	0.009	7.8	10.8	4.9	−9.2	−8.6	−9.8	−9.9	−9.3	−10.5
665	85.5	42,197	−6.8	−7.5	0.726	±	0.006	8.0	10.0	6.1	−9.0	−8.6	−9.4	−9.7	−9.3	−10.1
710	87.5	42,505	−6.9	−7.6	0.736	±	0.006	4.8	6.7	2.9	−9.8	−9.4	−10.2	−10.4	−10.0	−10.8
760	89.0	42,812	−7.1	−7.8	0.689	±	0.008	21.0	24.1	18.0	−6.8	−6.3	−7.4	−7.5	−6.9	−8.0
645	91.5	43,212	−7.1	−7.8	0.720	±	0.006	10.1	12.1	8.1	−8.9	−8.5	−9.3	−9.6	−9.2	−10.0

(*continued on next page*)

Table 1 (*continued*)

Analysis	Depth	Age	$\delta^{18}O_{OT02}$	$\Delta^{18}O_{OT02-SW}$	Δ_{47-ARF}			Δ_{47} temperature			$\delta^{18}O_{MW}$			$\Delta^{18}O_{MW-SW}$		
Number	(mm)	before A.D.	(‰ VPDB)	(‰ VPDB)	(‰)	±	SE	(°C)	Max	Min	(‰ VSMOW)	Max	Min	(‰ VSMOW)	Max	Min
698	92.5	43,612	−6.8	−7.4	0.723	±	0.006	9.0	11.0	7.1	−8.8	−8.4	−9.2	−9.4	−9.0	−9.8
677	93.5	44,012	−6.8	−7.4	0.732	±	0.006	6.0	8.0	4.1	−9.4	−9.0	−9.7	−10.0	−9.6	−10.4
563	94.5	44,412	−6.8	−7.5	0.723	±	0.009	9.1	12.1	6.1	−8.8	−8.2	−9.4	−9.4	−8.8	−10.0
734	96.5	45,444	−6.7	−7.3	0.729	±	0.008	7.0	9.6	4.4	−9.1	−8.6	−9.6	−9.7	−9.2	−10.3
627	99.0	46,477	−6.9	−7.4	0.726	±	0.006	8.0	9.9	6.0	−9.1	−8.7	−9.5	−9.6	−9.2	−10.0
691	103.0	48,842	−7.2	−7.8	0.719	±	0.006	10.2	12.2	8.2	−8.9	−8.5	−9.3	−9.6	−9.2	−10.0
538	105.0	50,175	−7.1	−7.6	0.705	±	0.009	15.4	18.6	12.2	−7.8	−7.2	−8.4	−8.4	−7.8	−9.0
670	106.5	51,043	−6.9	−7.5	0.716	±	0.006	11.4	13.5	9.4	−8.4	−8.0	−8.8	−9.0	−8.6	−9.4
715	108.0	51,911	−7.4	−7.9	0.722	±	0.006	9.5	11.5	7.5	−9.3	−8.9	−9.7	−9.8	−9.4	−10.2
560	109.5	52,779	−7.2	−7.7	0.725	±	0.009	8.3	11.3	5.4	−9.3	−8.7	−9.9	−9.9	−9.3	−10.5
646	110.5	53,442	−6.9	−7.5	0.719	±	0.006	10.5	12.5	8.5	−8.6	−8.2	−9.0	−9.2	−8.8	−9.6
702	112.0	54,104	−6.9	−7.4	0.728	±	0.006	7.5	9.4	5.5	−9.2	−8.8	−9.6	−9.7	−9.3	−10.1
547	113.0	54,767	−6.6	−7.2	0.746	±	0.009	1.5	4.3	−1.2	−10.2	−9.6	−10.7	−10.7	−10.1	−11.3
856	113.0	54,767	−6.7	−7.3	0.726	±	0.008	7.9	10.6	5.4	−9.0	−8.4	−9.5	−9.5	−9.0	−10.0
556	116.0	56,447	−7.0	−7.6	0.704	±	0.009	15.7	19.0	12.6	−7.7	−7.1	−8.3	−8.3	−7.7	−8.9
763	116.0	56,447	−7.0	−7.6	0.712	±	0.008	12.6	15.4	9.9	−8.3	−7.8	−8.9	−8.9	−8.4	−9.5
764	119.5	58,413	−7.3	−7.8	0.698	±	0.008	17.8	20.8	15.0	−7.6	−7.0	−8.1	−8.1	−7.6	−8.7
678	121.0	59,400	−7.4	−8.0	0.713	±	0.006	12.4	14.5	10.4	−8.8	−8.4	−9.2	−9.3	−8.9	−9.7
565	123.0	60,388	−7.6	−8.3	0.720	±	0.009	9.9	12.9	6.9	−9.4	−8.8	−10.0	−10.1	−9.5	−10.7
735	124.0	61,236	−7.4	−8.1	0.725	±	0.008	8.3	10.9	5.7	−9.6	−9.0	−10.1	−10.2	−9.7	−10.8
552	126.0	62,084	−6.6	−7.3	0.741	±	0.009	3.0	5.9	0.3	−9.8	−9.2	−10.4	−10.5	−9.9	−11.1
774	127.5	62,927	−6.8	−7.5	0.739	±	0.008	3.7	6.3	1.3	−9.9	−9.3	−10.4	−10.6	−10.1	−11.1

Tremaine et al. (2011); Eq. (2) as follows:

$$1000 ln\alpha_{water-calcite} = 16.1\left(10^3\ T^{-1}\right) - 24.6 \quad (2)$$

Eq. (2) was established for cave deposits (Tremaine et al., 2011) and is also consistent with $\delta^{18}O$ variability in Japanese stalagmites studied by Mori et al. (2018) and Kato et al. (2021). The temperature-dependent coefficient of $FT_{water-stalagmite}$ of Eq. (2) is approximately −0.19−−0.20‰/°C in the OT02 temperature range.

The index of past meteoric isotope, $\delta^{18}O_{MW}$ was calculated from $\delta^{18}O_{OT02}$ by following equation.

$$\delta^{18}O_{MW} = \left(1000 + \delta^{18}O_{OT02}\right)/\alpha_{water-calcite} - 1000 \quad (3)$$

$\delta^{18}O_{MW}$ principally refers to cave drip water, which is assumed to be almost the average value of meteoric water $\delta^{18}O$.

4. Results

4.1. Carbonate clumped isotope (Δ_{47}) temperature

The Δ_{47} values of 66 layers in OT02 range from 0.670‰ to 0.747‰ (Fig. 3d), corresponding to 1.4 °C–28.6 °C using Eq. (1) (Table 1). The overall trend of Δ_{47} variations broadly agrees with trend of $\delta^{18}O_{OT02}$ (Fig. 3). Comparatively high Δ_{47} values (low temperatures) were observed in portions in which less negative $\delta^{18}O_{OT02}$ values were observed. We found a positive correlation between $\delta^{18}O_{OT02}$ values normalized to seawater $\delta^{18}O$ change and Δ_{47} values of the OT02 stalagmite (discussed later in Sections 5.2 and 5.3).

The average Δ_{47} temperature of the Holocene portion (16.3 ± 5.6 °C, 8.8–2.6 ka) is 6.6 °C higher than the average of the lower portion (9.7 ± 4.6 °C, 63.5–34.8 ka) (Fig. 3d). The observed temperature drops corresponding to the HSs are 3 °C–5 °C. Interval of higher Δ_{47} temperatures, which presumably correspond to Hypsithermal event (Wanner et al., 2008) was during 5.4–3.8 ka (19.9 °C ± 6.0 °C) after a temporal cooling around 7 ka. Except for the warm period of Hypsithermal, the average Δ_{47} temperature during the Holocene is 14.1 °C ± 4.1 °C.

Smaller temperature variation of 1.8 °C–24.0 °C was calculated from the OT02 Δ_{47} range using the raft calibration (Affek and Zaarur, 2014; Matthews et al., 2021). The calculation results are shown in Table S2.

4.2. $\delta^{18}O_{MW}$ reconstruction

$\delta^{18}O_{MW}$ value vary between −10.3‰ and −6.2‰ (Table 1; Fig. 4e). The averaged $\delta^{18}O_{MW}$ value of the Holocene (8.8–2.6 ka) portion is less negative than that of the latest Pleistocene (63.5–34.8 ka) portion, as is the inverse trend of $\delta^{18}O_{OT02}$ value.

5. Discussion

5.1. Difference in climatic settings of Ohtaki and Maboroshi Caves

A major difference between the climatic settings of Ohtaki Cave (Nagataki) and Maboroshi Cave (Yuki) is a seasonal bias of precipitation amounts. In Nagataki, precipitation during the three winter months (December–February) accounts for 16.8% of annual precipitation and yearly variations in winter precipitation are much larger than those in Yuki (Figs. 2a and b). Consequently, the amount ratio of winter to annual precipitation is an important factor controlling the annual average $\delta^{18}O_{MW}$ values at Ohtaki Cave. On the other hand, in Yuki (near Maboroshi Cave), precipitation during the coldest 3 months (December–February) is limited to only 10% of the annual total and the yearly variation is also very limited in these months (Fig. 2b). The precipitation during the warmer 7 months (April–October) accounts for 78% of the annual total, which is more than three times the precipitation in the other 5 months (November–March; 22%) (Fig. 2b). In the region of

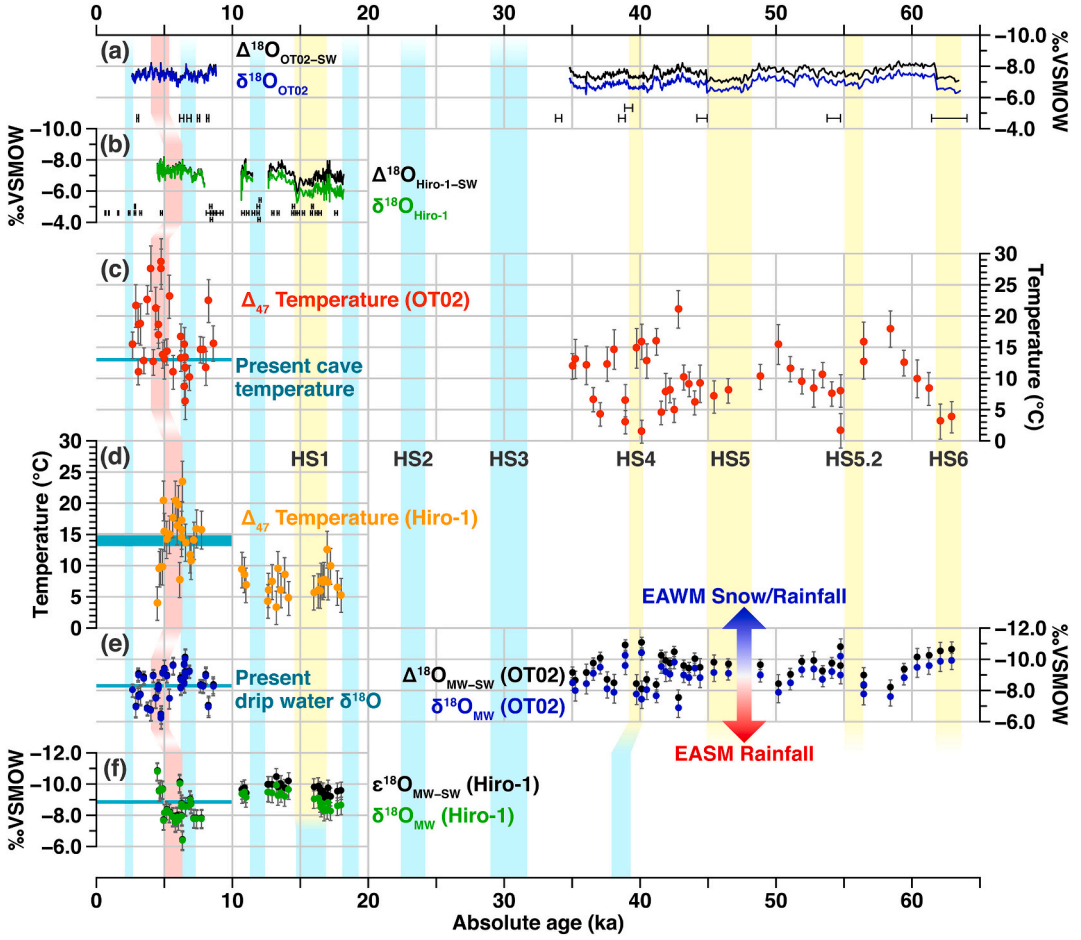

Fig. 4. (c) Δ_{47} temperature, (e) $\delta^{18}O_{MW}$ and $\Delta^{18}O_{MW-SW}$ from the OT02 stalagmite compared with (d, f) the results of the Hiro-1 stalagmite (Kato et al., 2021). The values of $\delta^{18}O_{MW}$ and $\Delta^{18}O_{MW-SW}$ for (e) OT02 and (f) Hiro-1 were calculated from (a) $\delta^{18}O_{OT02}$ and $\Delta^{18}O_{OT02-SW}$ and (b) $\delta^{18}O_{Hiro-1}$ and $\Delta^{18}O_{Hiro-1-SW}$, respectively, by the subtraction of temperature effect (Eqs. (3) and (6)) using (c, d) Δ_{47} temperatures. Yellow-vertical bands show the periods of Heinrich stadials. Light-blue bands show the periods of high lake level in Lake Nojiri, which occurs after heavy snowfall from EAWM as shown by Nakamura et al. (2013). The light-red band shows a period of warm climatic optimum corresponding to the Hypsithermal observed both in this study and in the Hiro-1 stalagmite of Kato et al. (2021). (For interpretation of the references to colour in this figure legend, the reader is referred to the web version of this article.)

Maboroshi Cave, the Chugoku Mountains (1729 m asl) obstruct the winter rain/snowfall from the Japan Sea side. It is therefore estimated that the amount ratio of winter and annual precipitation has less importance for the annual average $\delta^{18}O_{MW}$ values at Maboroshi Cave.

The depths of surrounding seas caused another difference in hydrological settings in a millennial scale. The SIS (Fig. 1b) is currently shallow (mostly <50 m deep) and is an important vapor source for Maboroshi Cave in Hiroshima. However, the SIS was almost exposed during the glacial sea-level low. Because of the absence of this inland sea, moisture was predominantly transported over longer distances from the marine vapor source. Less negative $\delta^{18}O_{MW}$ from the SIS was established by the Holocene glacial retreat (Kato et al., 2021). By contrast, the influence of the SIS is negligible for Ohtaki Cave in Gifu prefecture (Fig. 1b).

5.2. Stable oxygen isotope compositions normalized to seawater values

We corrected $\delta^{18}O_{OT02}$ values by removing variations in the marine $\delta^{18}O$ following the assumption and method by Mori et al. (2018). Stalagmite $\delta^{18}O_C$ changes with drip water $\delta^{18}O$ derived from meteoric $\delta^{18}O$ ($\delta^{18}O_{MW}$). Although the $\delta^{18}O_{MW}$ is determined via various processes, such as evaporation from seawater, moisture transfer, condensation, and precipitation, it must be controlled by the $\delta^{18}O$ of seawater ($\delta^{18}O_{SW}$), which is the dominant moisture source in the Japanese Islands. The oxygen isotope values of drip water and OT02 ($\delta^{18}O_{OT02}$) were influenced by changes in $\delta^{18}O_{SW}$, according to their hypothesis. We accounted for the influence from $\delta^{18}O_{SW}$ change ($\Delta^{18}O_{SW}$) according to Mori et al. (2018) to correct the $\delta^{18}O_{OT02}$ values for the $\delta^{18}O_{SW}$ change, as follows:

$$\Delta^{18}O_{SW} = \left(\delta^{18}O_{foram} - 3.26\right) \times 1/(5.03–3.26) \quad (4)$$

where $\delta^{18}O_{foram}$ is the time series from deep Pacific benthic forams reported for the last glacial cycle (150 kyr) by Lisiecki and Stern (2016). Their data, which is standardized for every 500 years, exhibit variations ranging from +5.03‰ during the LGM to +3.26‰ in the Holocene. Although their $\delta^{18}O_{foram}$ represents the fluctuation in deep water $\delta^{18}O_{SW}$, it differs very slightly from the value of surface water. However, the $\delta^{18}O_{foram}$ reflects the combined signals of $\delta^{18}O_{SW}$ and ocean temperature. Eq. (4) converts $\delta^{18}O_{foram}$ to $\Delta^{18}O_{SW}$ (Fig. 3b) following the assumption that ^{18}O enrichment in seawater during the LGM was 1.0‰ ± 0.1‰ (Schrag et al., 1996, 2002; Bintanja and van de Wal, 2008; Shakun et al., 2015). We follow Mori et al. (2018) in defining the residual variation in $\delta^{18}O_{OT02}$ by subtracting the influence from $\delta^{18}O_{SW}$ change ($\Delta^{18}O_{SW}$) as follows:

$$\Delta^{18}O_{OT02-SW} = \delta^{18}O_{OT02} - \Delta^{18}O_{SW} \text{ (in VPDB scale)} \quad (5)$$

We then assume that residual variation ($\Delta^{18}O_{OT02-SW}$) reflects

variations in hydrologic processes (e.g., fractionation from seawater to vapor, amount effect, and continental effect on meteoric $\delta^{18}O$) and signals of deposition temperature (temperature-dependent fractionation between water and calcite). $\Delta^{18}O_{OT02-SW}$ shows a small variation between −8.3‰ and −6.7‰ and most values fall between −7‰ and −8‰ (Fig. 3c). No significant difference was observed between the averaged $\Delta^{18}O_{OT02-SW}$ values of the latest Pleistocene (63.5–34.8 ka) and the Holocene (8.8–2.6 ka) (Fig. 3c).

In addition to $\delta^{18}O_{MW}$, we defined another index of past meteoric isotope, $\Delta^{18}O_{MW-SW}$, which was calculated from $\Delta^{18}O_{OT02-SW}$ by following equation.

$$\Delta^{18}O_{MW-SW} = \left(1000 + \Delta^{18}O_{OT02-SW}\right)/\alpha_{water-calcite} - 1000 \quad (6)$$

$\Delta^{18}O_{MW-SW}$ refers to the difference between $\delta^{18}O_{MW}$ and $\delta^{18}O_{SW}$; in other words, the total fractionation in the hydrologic circulation process (from seawater to meteoric water) involving changes in climatic factors including the monsoon intensity, moisture trajectory, and the seasonality of precipitation. $\Delta^{18}O_{MW-SW}$ value varies between −11.0‰ and −6.2‰ (Table 1; Fig. 4e).

5.3. Discrimination of KIEs and temperature calibration for OT02 Δ_{47}values

Before paleoclimatic reconstruction, we inspected the reliability of our results as paleoclimatic records. In principle, both calcite $\delta^{18}O$ and Δ_{47} values decrease with temperature rise. If temperature variation is the dominant control on calcite $\delta^{18}O$ and Δ_{47} values, they should positively correlate. Nevertheless, these temperature dependencies can be complicated by the KIE due to precipitation-driven CO_2 degassing from the parent water. It has been suggested that CO_2 degassing elevates $\delta^{18}O$ values and lowers Δ_{47} values of carbonate minerals by incomplete isotopic exchange among water and DIC species (Guo, 2008; Daëron et al., 2011; Kluge and Affek, 2012; Guo and Zhou, 2019; Dreybrodt and Fohlmeister, 2022) and can generate isotopic offsets (differences between actual and equilibrium values). Some speleothems show a

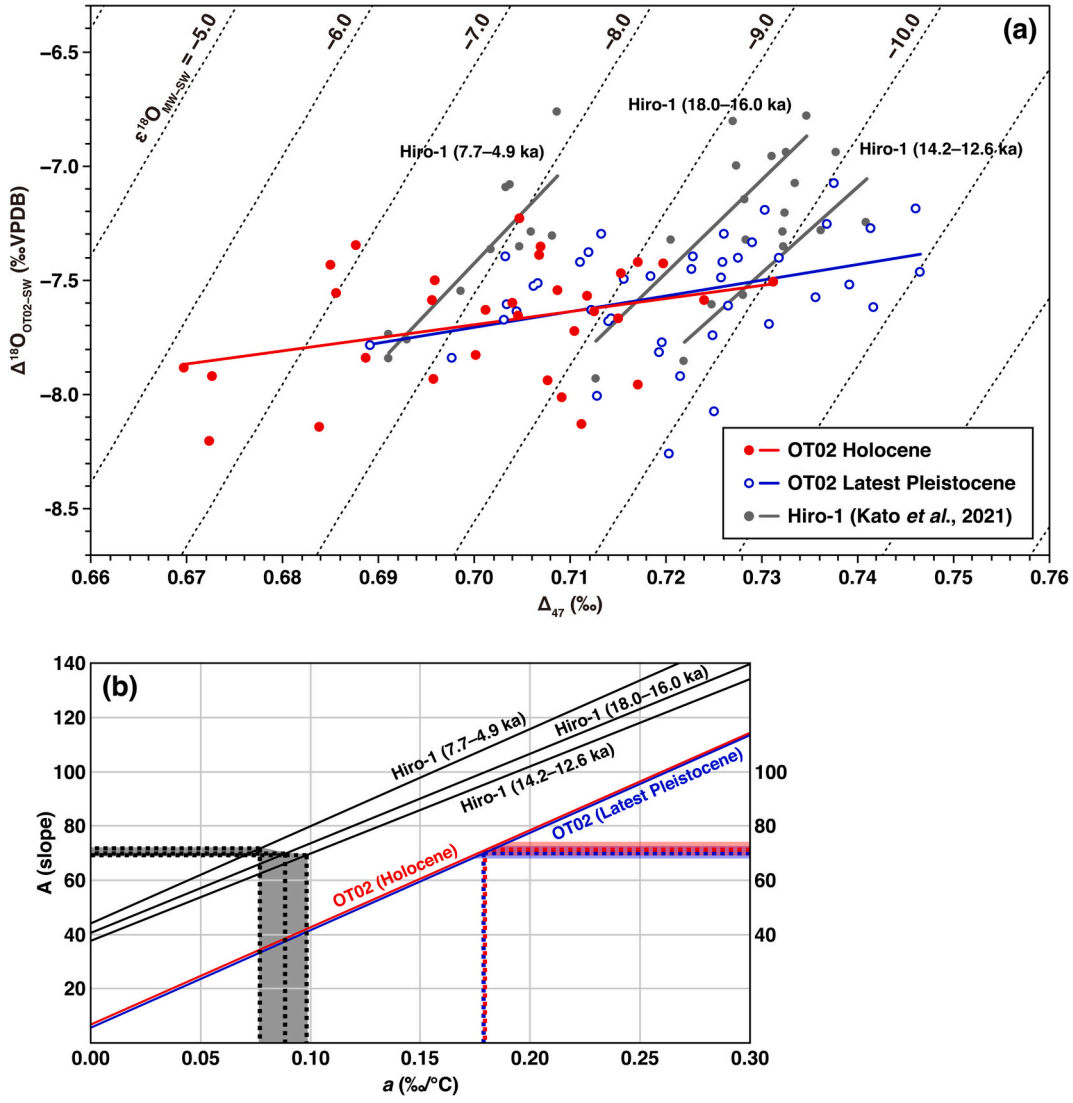

Fig. 5. (a) Cross-plot of OT02 Δ_{47} and $\Delta^{18}O_{OT02-SW}$. Dashed lines show the theoretical relationships at stable $\Delta^{18}O_{MW-SW}$ values from −13.0‰ to −4.0‰ (VSMOW) calculated using Eqs. (2) and (5) (Kato et al., 2019; Tremaine et al., 2011).
The regression lines of OT02 are given for the Holocene (in red) and latest Pleistocene (in blue) and they are indistinguishable from each other. The slopes of these lines are clearly shallower than the theoretical relationships and the three discrete regression lines for the Hiro-1 stalagmite (Kato et al., 2021). (b) Slopes of regression lines (A in Eq. (6)) between Δ_{47} and ($\Delta^{18}O_{OT02-SW}$ − FT_{SW-MW}) under the variable temperature dependency of FT_{SW-MW} (a in Eq. (7)). The a value for OT02 is 0.18 (‰/°C), which is clearly larger than that for Hiro-1, 0.08–0.10 (‰/°C; Kato et al., 2021). (For interpretation of the references to colour in this figure legend, the reader is referred to the web version of this article.)

negative correlation between $\delta^{18}O$ offset and Δ_{47} offset (Daëron et al., 2011; Wainer et al., 2011; Kluge and Affek, 2012; Kluge et al., 2013; Affek et al., 2014). This type of covariation (negative correlation) between $\delta^{18}O$ and Δ_{47} offsets develops when KIE fractionation significantly affects $\delta^{18}O$ and Δ_{47}. In such cases, Δ_{47} temperature is unusable for paleoclimatic reconstruction.

We examined the covariation between $\Delta^{18}O_{OT02-SW}$ and Δ_{47} values of the OT02 stalagmite to distinguish the influences from temperature and KIE. Here, we use $\Delta^{18}O_{OT02-SW}$ rather than $\delta^{18}O_{\ OT02}$ because the $\Delta^{18}O_{OT02-SW}$ is better index of temperature considering $\delta^{18}O_{SW}$ change ($\Delta^{18}O_{SW}$). In the OT02 stalagmite, a weak but positive covariation between $\Delta^{18}O_{OT02-SW}$ and Δ_{47} values was observed and expressed as Eq. (7) (Fig. 5a, r = 0.42, $n = 74$, $p < 0.01$).

$$\Delta^{18}O_{OT02-SW} = 6.35\ \Delta_{47} - 12.14\ \left(n = 74, R^2 = 0.177, p < 0.01\right) \quad (7)$$

This regression of Δ_{47} versus $\Delta^{18}O_{OT02-SW}$ is common to the Holocene and the latest Pleistocene intervals, which have difference in the temperature range (Fig. 5a). The weakness of this correlation can be due to variations in $\delta^{18}O_{MW}$ and KIE strength, and deviations in Δ_{47} measurment of ±0.006‰–0.009‰. However, the positive relationship supports the hypothesis that the signals, Δ_{47} and $\Delta^{18}O_{OT02-SW}$ are not largely disturbed by changes in the strength of KIE disequilibrium, and that temperature and temperature-dependent changes are the principal factors controlling both the overall trends of Δ_{47} and $\Delta^{18}O_{OT02-SW}$.

For the purpose of comparison, in the case of the Hiro-1 stalagmite, the positive covariation was found also in most parts of the stalagmite, supporting the interpretation that both Δ_{47} and $\delta^{18}O_{Hiro\text{-}1}$ changed mainly with temperature (Kato et al., 2021). However, several layers of low growth rate and less negative $\delta^{13}C$ in Hiro-1 which imply dry conditions and high PCP (Hori et al., 2013) exhibited features of the strong influence of KIE disequilibrium: less negative $\delta^{18}O$ values and smaller Δ_{47} values.

The growth rate of the OT02 stalagmite is higher and more stable (around 1–4 μm/yr in the latest Pleistocene portion and 8–9 μm/yr in the Holocene portion) than that of the Hiro-1 stalagmite (<0.3 μm/yr in HS1 and up to 3–4 μm/yr in 6.0–6.5 and 16.5–17.0 ka; Hori et al., 2013; Kato et al., 2021). Additionally, subsamples for Δ_{47} measurements were collected from clear layers of OT02 excluding opaque/muddy horizons to avoid the effect of KIE as much as possible, as mentioned in Section 3.1.1. A stable growth rate is likely the reason for absence of strong KIE disequilibrium in the OT02 stalagmite. Therefore, we deduce that temperature is the dominant control on the OT02 Δ_{47} record and that the relationship is consistent throughout the growth of OT02 from the latest Pleistocene to the middle Holocene. Further, the average Δ_{47} temperature during the Holocene, except for the Hypsithermal warm period (14.1 °C ± 4.1 °C), is identical with the current cave temperature of 13.0 °C within the uncertainty. Therefore, the temperature reconstruction using tufa calibration (Eq. (1); Kato et al., 2019) appears to be successful.

5.4. Terrestrial paleotemperature

We interpret temperature to be the dominant and consistent control on the OT02 Δ_{47} record, on the basis of the discussion presented in Section 5.3. The Δ_{47} temperature record from OT02 (Table 1) is also broadly consistent with known climatic stages, such as cooling during HS6 and cooling around HS5.2, warming during the Holocene, and a warming peak around the Hypsithermal event (9 to 6–5 ka; Wanner et al., 2008), although the cooling in HS5 is not so significant comparing to HS6 and HS5.2 and Δ_{47} temperature show large scatter during HS4 (±6.0 °C) and the warming peak of the Hypthithermal (±6.2 °C) (Fig. 4c). In the period common to the OT02 and Hiro-1 stalagmites (7.7–4.5 ka), the two stalagmites exhibit very similar patterns in Δ_{47} temperature (Figs. 4c and d); a rapid warming in 7.0–6.0 ka after a temporal cooling of about 5 °C at 7.0 ka from around 15 °C at 8.0–7.5 ka and a gradual cooling to the cessation of stalagmite growth. Notably, the data plots of OT02 were calibrated to the age of Hiro-1 by the shapes of Δ_{47} fluctuations with red vertical bars in Fig. 4, considering the larger dating error for OT02 (up to ±2.5 kyr) aforementioned. For the same reason, H5.2 cooling is thought to be responsible for the comparatively low Δ_{47} temperatures observed around 54.8–54.1 ka of OT02 U-Th age. Thus, three distinct and venial cooling intervals of 3 °C–5 °C are likely linked to HS6, HS5.2, and HS5 (Fig. 4c). Although the averaged Δ_{47} temperature of the latest Pleistocene portion of OT02 (63–35 ka) is lower than that of the Holocene portion, the Δ_{47} temperature in warm periods between each Heinrich stadial reached 10 °C–15 °C, which is as high as the present temperature and the average of the Holocene.

Our Δ_{47} temperature equation (Eq. (1)) was calibrated using the Δ_{47} values of natural tufa deposited at 5.6 °C–16.0 °C. The high Δ_{47} temperatures over 20 °C around 5.4–2.9 ka therefore somewhat deviate from the temperature range covered by Eq. (1). Because of the nature of carbonate clumped isotope thermometry, the uncertainty of Δ_{47} temperatures is greater at higher temperatures, because the Δ_{47} value exhibits an inverse proportionality to the square of the temperature in Kelvins. Even after considering these larger errors and uncertainties, the average temperature during the period from 5.4 to 3.8 ka (considering the larger dating error for OT02 mentioned above, which likely corresponds to the warm maximum of 6.3–4.9 ka recorded in Hiro-1) is 19.9 °C ± 6.0 °C and is higher than the present cave temperature of 13 °C.

Seasonal temperature variation is currently very limited (presumably within ±1.0 °C) in the deeper part of Ohtaki Cave, and it is thus likely that the past cave temperature was also stable on seasonal timescales. The high-average Δ_{47} temperature during the Hypsithermal does not necessarily mean uniform warming of all seasons. In Nagataki (near Ohtaki Cave), the temperature variation tends to be largest in the colder season (November–April) and smaller in the warmer season (May–October; Fig. 6a). The correlation coefficient (R) of annual and monthly temperatures is large in February–May and September–October and smallest in the warmest months (July–August; Fig. 6a). Together, this indicates that summer temperature is not an important control in the determination of annual average temperatures. Variability in annual average temperature is largely dependent on temperature variability in spring and autumn and is also somewhat dependent on winter temperature. Though the assumption cannot be proven by our stalagmite records, we raise the possibility that the annual average temperature in Nagataki is characterized by the lengths of the warmer time and the colder time of year. Based on the assusmption, the higher cave temperature of 19.9 °C ± 6.0 °C observed in the 5.4–3.8 ka period of OT02 (corresponding 6.3–4.9 ka of Hiro-1) was possibly induced by longer high summers and shorter winters than at present, accompanied by the warm climate optimum of the Hypsithermal event.

5.5. Features in the correlation between Δ_{47}versus $\Delta^{18}O_{OT02-SW}$

A unified regression of Δ_{47} versus $\Delta^{18}O_{OT02-SW}$ was obtained for the OT02 stalagmite from the latest Pleistocene and also from the middle Holocene (Eq. (7)). However, the slope of 6.35 is significantly shallower than that of the hypothetical relationship (A*). Where both stalagmite $\delta^{18}O_C$ and Δ_{47} are solely controlled by depositional temperature (in other words, assuming a constant drip water $\delta^{18}O_W$), the relationship between $\delta^{18}O_C$ and Δ_{47} can be theoretically calculated. We applied the temperature dependency of Δ_{47} (Eq. (1)) and $\delta^{18}O$ (Eq. (2); Tremaine et al., 2011). The hypothetical relationship between Δ_{47} and $\Delta^{18}O_{stalagmtie-SW}$ is almost linear, with a slope A* around 70, but is slightly dependent on the Δ_{47} value (i.e., temperature) (approximately 72.5 at $\Delta_{47} = 0.69$, 68.5 at $\Delta_{47} = 0.74$).

The temperature dependency of meteoric water $\delta^{18}O_{MW}$ was viewed as a possible cause for the shallower slope. The apparent positive links between local surface air temperature and the meteoric $\delta^{18}O_{MW}$ have been reported globally (Dansgaard, 1964; Rozanski et al., 1993). This

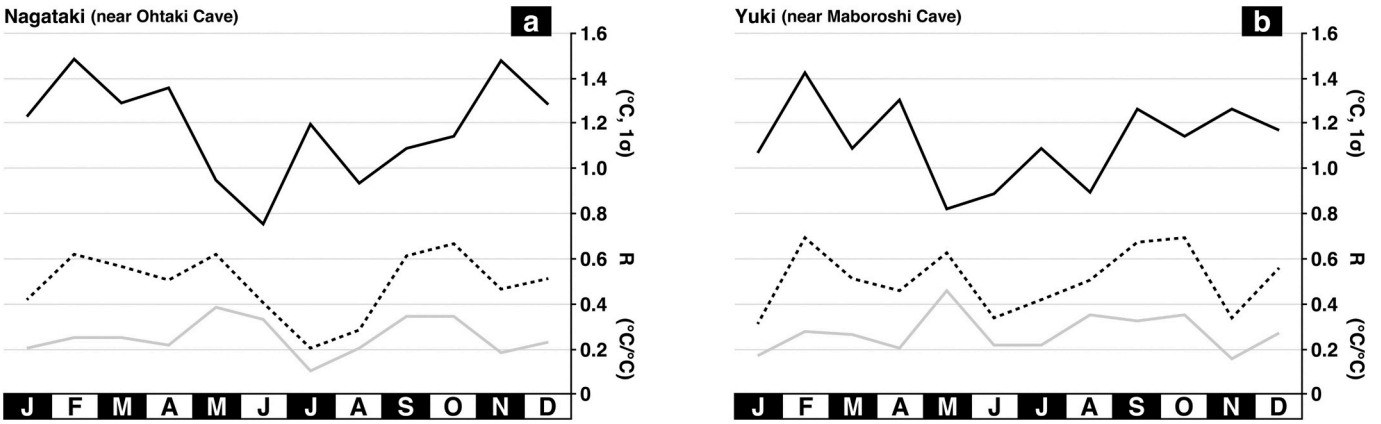

Fig. 6. Relationship between monthly and annual mean temperatures in (a) Nagataki and (b) Yuki based on data for the period 1981–2020. Black lines show standard deviations in monthly mean temperature (1σ). Dashed lines show the correlation coefficient (R) between monthly and annual mean temperatures. Gray lines show the impacts of monthly temperatures on the annual average (°C /°C).

relationship can be explained using the renowned Craig-Gordon-type model of isotopic fractionation during water evaporation and the Rayleigh-type fractionation model during water condensation. It appears reasonable that $\delta^{18}O_{MW}$ would be less negative in a temperate climate. To evaluate this interpretation, we defined the temperature-dependent fractionation from seawater to meteoric water as FT_{SW-MW} (in ‰) and expressed the relationships between Δ_{47} and $\Delta^{18}O_{C\ (OT02\ or\ Hiro\text{-}1)-SW}$ as shown in Eqs. (8) and (9):

$$a = dFT_{SW-MW}/dT \tag{8}$$

$$\Delta^{18}O_{C\ (OT02\ or\ Hiro-1)-SW} = A\Delta_{47} + FT_{SW-MW} + B \tag{9}$$

where T is the local surface air temperature in °C and FT_{SW-MW} is assumed to be a linear function of T in a limited temeptature range. The temperature-dependent coefficient of FT_{SW-MW} is expressed by a (‰/°C). The slope A in Eq. (9) increases with the a of Eq. (8) and reaches the hypothetical slope A* of Δ_{47} versus $\Delta^{18}O_{stalagmtie-SW}$ (approximately 70 as mentioned above) when a takes an appropriate value (Fig. 5b). In the OT02 stalagmite, the slope A reaches the hypothetical value A* when a_{OT02} is at 0.18‰/°C for both the Holocene and latest Pleistocene (red line for the Holocene and blue line for the latest Pleistocene in Fig. 5b).

The regression of OT02 Δ_{47} versus $\Delta^{18}O_{OT02-SW}$ (Eq. (7); Fig. 5a) and the a_{OT02} value (0.18‰/°C) are common to the Holocene and the latest Pleistocene intervals of OT02, but different in the Hiro-1 stalagmite. In the case of the Hiro-1 stalagmite, different regressions of Δ_{47} versus $\Delta^{18}O_{Hiro\text{-}1-SW}$ were obtained from three discrete periods, 18.0–16.0, 14.2–12.6, and 7.7–4.9 ka (Fig. 5a, Kato et al., 2021). An especially large difference was noted between regressions in the pre-Holocene and mid-Holocene. Kato et al. (2021) explained this discrepancy in regressions by differences in meteoric water $\delta^{18}O_{MW}$ ($\Delta^{18}O_{MW-SW}$) due to the presence or absence of the SIS (Fig. 1b), which is an important vapor source for Maboroshi Cave in Hiroshima when the sea level was high. Less negative $\delta^{18}O_{MW}$ from the SIS was established by the Holocene glacial retreat (Kato et al., 2021). By contrast, the influence of the SIS is negligible for Ohtaki Cave in Gifu prefecture (Fig. 1b). This is likely the reason for the unified regression of Δ_{47} versus $\Delta^{18}O_{OT02-SW}$ (Eq. (7)) for Ohtaki Cave (Fig. 5a).

There is another characteristic in the regression slopes of OT02 Δ_{47} versus $\Delta^{18}O_{OT02-SW}$ compared to Hiro-1 values. The regression slope 6.35 of OT02 (Eq. (7)) is shallower than those of the Hiro-1 stalagmite which are approximately 40 (37.71–44.15; Kato et al., 2021) (Fig. 5a). Fig. 5b also shows the calculation results of $a_{Hiro\text{-}1}$ (black lines in Fig. 5b; Kato et al., 2021). The differences in these slopes are thought to be the result of distinct temperature dependencies of meteoric $\delta^{18}O_{MW}$ between these two cave sites. In the Hiro-1 stalagmite, Slope A in Eq. (8) reaches the hypothetical slope A* when $a_{Hiro\text{-}1}$ is at 0.077‰–0.098‰/°C (black lines in Fig. 5b; Kato et al., 2021), which is smaller than a_{OT02}.

5.6. Reason for the larger temperature-dependent coefffcient of FT_{SW-MW}(*a*) *in OT02*

We assume that the divergence in a values for OT02 and Hiro-1 are ascribed to regional differences in precipitation characteristics. As described in Section 2.3, in both Nagataki (near Ohtaki Cave; Fig. 2c) and Yuki (near Maboroshi Cave; Fig. 2d), less negative $\delta^{18}O_{MW}$ values are observed during the warm season, whereas more negative $\delta^{18}O_{MW}$ values are observed in the cold season. However, in Nagataki, winter precipitation accounts for a larger proportion (16.8%) of the annual total, and the yearly variation of winter precipitation is twice or three times as large as that in Yuki (Figs. 2a and b). Hence, the amount ratio of winter/annual precipitations is an important factor influencing the annual average $\delta^{18}O_{MW}$ values at Ohtaki Cave.

The major control of winter precipitation from the Japan Sea side is the strength of the EAWM. Hirose and Fukudome (2006) found a significant correlation ($R^2 = 0.85$) between the average winter precipitation on the Japan Sea side of Honshu and Hokkaido islands in 1907–2006 and the winter monsoon index of Hanawa et al. (1988), which reflects differences in the sea-level pressures between Irkutsk and Nemuro in winter and represents the strength of the EAWM. Hirose and Fukudome (2006) also found that the Japan Sea SST in winter (November–January) exhibited a significant correlation with winter precipitation on the Japan Sea side ($R^2 = 0.82$). This relation occurs because the high SST of the Japan Sea increases evaporation from seawater, which is the supply source of winter snow/rainfall to Japan. In the Northwest Pacific and East Asia, the land–sea thermal contrast is a driving force behind both the EASM and EAWM. As described above, the proportion of winter/summer precipitation is more variable in the Ohtaki region and the proportion is largely dependent on winter precipitation. Cooling of the land area results in increased winter precipitation and decreased annual average $\delta^{18}O_{MW}$ values in Ohtaki. This is likely the reason for the apparently larger temperature dependency of meteoric water $\delta^{18}O_{MW}$ expressed by a (0.18 ‰/°C) in the Ohtaki region.

5.7. Paleoprecipitation history

In Section 5.4, we raised an assumption that the changes in cave temperature were arising from interactions between the warmer season and the colder season of year. In Japan, summer and winter climates are characterized by the EASM and EAWM winds, respectively (Fukui, 1977). Generally in the Pacific side of Japan except for south-west

islands, winter rain/snowfall has a $\delta^{18}O_{MW}$ value more nagtive than summer rainfall with two peaks of $\delta^{18}O_{MW}$ in spring and autumn (Tanoue et al., 2013). This pattern was also observed in Nagataki and typically in Yuki (Figs. 2c and d). Changes in summer and winter durations might therefore affect the precipitation balance between summer and winter which are intimately connected to EASM and EAWM winds, and consequently determine the annual average of $\delta^{18}O_{MW}$ value. Based on this assumption, paleometeoric water should have a more negative $\delta^{18}O_{MW}$ value in colder periods and a less negative $\delta^{18}O_{MW}$ value in warmer periods. However, the relation between EASM and EAWM is not simple as stated below. Previous paleoclimatic studies have indicated numerous relationships between the intensities of EASM and EAWM: an inverse correlation (Xiao et al., 1995; Yancheva et al., 2007; Liu et al., 2009), a positive correlation (Zhang and Lu, 2007), and both positive and inverse correlations depending on the period and timescale concerned (Steinke et al., 2011; Ge et al., 2017), although these studies were performed from the Tibetan–Chinese continental regions and surrounding seas. Recently, Yan et al. (2020) presented simulation results to investigate the relationship between time series changes in EASM and EAWM, showing that their intensities are positively correlated at orbital timescale due to seasonal insolation forcing but are negatively correlated over multidecadal to millennial timescales, primarily as a result of internal variability in the Atlantic Meridional Overturning Circulation and its subsequent teleconnection to East Asia via land–sea thermal contrasts.

Focusing on climatic changes at the centennial–millennial timescale, i.e., HSs and Hypsithermal warming, the results of our meteoric water $\delta^{18}O_{MW}$ and $\Delta^{18}O_{MW-SW}$ reconstruction are consistent with the assumption of a more negative $\delta^{18}O_{MW}$ value in colder periods, such as HSs and the period of cooling around 7 ka, and less nergative in warmer preiods (Fig. 4e). This is consistent with the assumption in Section 5.4 that the longer durations of the warmer season and higher amounts of EASM rainfall increased the average $\delta^{18}O_{MW}$ value in the Hypsithermal warm period. By contrast, it is presumed that EAWM brought a higher amount of snow and rainfall during the long colder season to Ohtaki Cave during HSs. The Hypsithermal (also known as the Holocene climatic optimum) is a warming period in northern mid to high latitudes (Wanner et al., 2008) that was commonly defined by the peak of EASM rainfall in Chinese continental regions (An et al., 2000). In Chinese continental regions, Heinrich stadials (HSs1–6) were involved in the EAM changes, the weak EASM, and the strong EAWM (Porter and An, 1995; Wang et al., 2001; Song et al., 2018). In comparison with the results from Chinese continental regions, our estimation results of higher amounts of EASM rainfall in the Hypsithermal warm period and higher amounts of EAWM snow/rainfall during HSs in the Ohtaki region appear credible. Although our results are based on changes in EASM/EAWM durations rather than their strengths, the intensity and duration of EASM are found to be positively coreretive in China in recent decades (Li et al., 2021). It is realistic to believe that the duration and strength of EASM/EAWM are positively related at the centennial–millennial timescale. The strong and/or long-lasting EAWM in Heinrich stadial results in a dry winter in Chinese continental regions (Porter and An, 1995; Wang et al., 2001; Song et al., 2018). However, EAWM is an important moisture source for Japan in the winter. We presume that the strong and/or long-lasting EAWM would result in a wet winter in the Japan Sea side in HSs. However, only a few prior investigations from Japan have reported terrestrial climatic records in HSs. Nakamura et al. (2013) performed stratigraphic analyses of acoustic records of sediments in Lake Nojiri, the Japan Sea side of central Japan (Fig. 1b) where winter snowfall accounts for approximately 30% of annual precipitation. They revealed lake level fluctuation during the past 45,000 years and found eight sets of rising and falling levels, although their results contain large dating errors of ±1000–15,000 years. They also found that peaks of lake level corresponded to cold climate stages such as HSs1–4 and the Younger Dryas. They presumed that lake level rises were caused by increased snowfall from an enhanced winter monsoon (EAWM). Light blue vertical bands in Fig. 4 indicate the periods of peak lake level in Nojiri identified by Nakamura et al. (2013). Unfortunately, the record of Nakamura et al. (2013) does not include older HSs5–6, for which particularly negative $\Delta^{18}O_{MW-SW}$ values were reconstructed from OT02 (Fig. 4e). However, the durations of high lake level periods in Nojiri seem to correspond to the periods of colder temperature and more negative $\Delta^{18}O_{MW-SW}$ values (HS4 and a temporal cooling around 7 ka). Increased precipitation from EAWM was likely also bought into the Ohtaki region and caused a decrease in the annual average of $\Delta^{18}O_{MW-SW}$ during these cold stages.

As described here, changes in the amount ratio of summer (warmer season) and winter (colder season) precipitations from EASM and EAWM caused the divergence in $\Delta^{18}O_{MW-SW}$ values in the Ohtaki region, although the temperature dependency of the fractionation between seawater and meteoric water (as discussed in Section 5.6) also accounts for the relationship between temperature and $\Delta^{18}O_{MW-SW}$. The relation that less/more negative meteoric $\delta^{18}O_{MW}$ in warmer/colder climate stages is the opposite to the conventional assumption that meteoric $\delta^{18}O_{MW}$ becomes more/less negative in warm–humid/cold–dry climates due to the so-called "amount effect."

As described in Section 5.1, precipitation from EAWM is minor in the region of Maboroshi Cave. We suggest that a strong EAWM and weak EASM during cold periods caused the dry conditions of Maboroshi Cave, which might have resulted in the interruptions of the growth of Hiro-1 and KIE disturbance of Hiro-1 records (Figs. 4b and d).

6. Summary

We analyzed carbonate clumped isotopes (Δ_{47}) of the OT02 stalagmite from Ohtaki Cave and revealed changes in terrestrial temperature and meteoric $\delta^{18}O$. The average Δ_{47} temperature of the Holocene portion (16.3 °C, 8.8–2.6 ka) is 6.6 °C higher than that of the latest Pleistocene portion (9.7 °C, 63.5–34.8 ka). Decrease in Δ_{47} temperature correspond to HSs and are approximately 3 °C–5 °C. We presume that higher cave temperatures of 19.9 °C ± 6.0 °C observed during the middle Holocene (5.4–3.8 ka of OT02) were induced by longer high summers and shorter winters than at present, accompanied by the Hypsithermal warm climate optimum.

We also reconstructed two indices of meteoric oxygen isotopes, $\delta^{18}O_{MW}$ and $\Delta^{18}O_{MW-SW}$, by subtracting the temperature effect from $\delta^{18}O_{OT02}$ and $\Delta^{18}O_{OT02-SW}$. The averaged $\delta^{18}O_{MW}$ and $\Delta^{18}O_{MW-SW}$ values through the Holocene (8.8–2.6 ka) portion are less negative than those of the latest Pleistocene (63.5–34.8 ka) portion. Focusing on climatic changes at centennial–millennial timescale, $\Delta^{18}O_{MW-SW}$ values (and accordingly $\delta^{18}O_{MW}$ values) were more negative in colder periods, such as HSs and the cooling event around 7 ka, and less negative in warmer periods such as the Hypsithermal. These relationships indicate the coevolution of terrestrial paleotemperature and paleoprecipitation. Increased precipitation brought by EASM has likely increased the average $\delta^{18}O_{MW}$ in warmer periods such as the Hypsithermal, whereas increased precipitation brought by EAWM has decreased the averaged $\delta^{18}O_{MW}$ in colder periods such as HSs. Besides, we presume that seasonal precipitation distributions are also affected by global warming/cooling conditions; during periods of global warming, long-lasting EASM brings more precipitation to the Pacific side of Japan. However, long-lasting EAWM brings more rain/snowfall to the Japan Sea side during periods of global cooling.

Hence, we revealed a trend of more/less negative meteoric $\delta^{18}O_{MW}$ in warmer/colder climate stages. This trend is the opposite of that assumed in conventional stalagmite paleoclimate studies, which suggest that meteoric $\delta^{18}O_{MW}$ becomes more negative in warm–humid climates due to the "amount effect." Our results also do not follow previous interpretations that variation in meteoric $\delta^{18}O_{MW}$ values is the dominant controlling factor of stalagmite $\delta^{18}O$ value. In our study regions, major factors determining the average $\delta^{18}O_{MW}$ value are 1) the proportion between summer and winter precipitation and 2) the temperature dependency of the fractionation from seawater to meteoric water.

Additionally, 3) seawater $\delta^{18}O_{SW}$ change ($\Delta^{18}O_{SW}$) at orbital scales also influences $\delta^{18}O_{MW}$. These effects occur due to the hydrological setting in Japan in which moisture is brought from surrounding seas. Factor 1 is related to climatic stages on centennial scales, which is also deeply related to terrestrial temperature. Besides these three factors controlling $\delta^{18}O_{MW}$, 4) temperature-dependent fractionation at the time of stalagmite deposition ($FT_{water-stalagmite}$) is an important control on stalagmite $\delta^{18}O_C$ (approximately −0.19−−0.20‰/°C). These temperature effects on $\delta^{18}O_{MW}$ (0.18‰/°C of facors 1 and 2) and $\delta^{18}O_C$ (factor 4) are, however, in opposite directions and the negative influence of temperature on $\delta^{18}O_C$ (factor 4) exceeds the information available for past $\delta^{18}O_{MW}$. This explains the small amplitude of $\delta^{18}O$ change in Japanese stalagmites (Mori et al., 2018; Kato et al., 2021) and has complicated the interpretation of stalagmite $\delta^{18}O_C$ records using only conventional methods of stalagmite climatology depending only on $\delta^{18}O$ analysis.

Funding

This study was supported by Grants-in-Aid from the Japan Society for the Promotion of Science [70782019, 20J00843, and 21K18393 for HK, and 16H02235 and 20H00191 for AK] and partially supported by grants from the Science Vanguard Research Program of the Ministry of Science and Technology (MOST) (110-2123-M-002-009), the National Taiwan University (109L8926 to C-CS), the Higher Education Sprout Project of the Ministry of Education (110L901001 and 110L8907), Taiwan ROC for C-CS.

Authors' contributions

The study was conceptualized, designed, and proposed by HK. The experiment was conducted by HK, TM, AK, C-CW, and C-CS. This study's manuscript was written by HK and AK. The study was supervised by AK and C-CS. The final manuscript was read and approved by the authors.

Declaration of Competing Interest

The authors declare that they have no competing interest.

Data availability

Table 1 contains all of first appearance data in this study.

Acknowledgment

Weather data and bathymetric data in this study are from the Japan Meteorological Agency (http://www.jma.go.jp) and the NOAA National Geophysical Data Center, 2009: ETOPO1 1 Arc-Minute Global Relief Model (Accessed in July 2021). We thank Yoshihiro Kuwahara and Ryoko Senda (Kyushu University) for supporting the Δ_{47} analysis. We thank anonymous reviewers for suggestions and edits that largely improved this manuscript.

Appendix A. Supplementary data

Supplementary data to this article can be found online at https://doi.org/10.1016/j.chemgeo.2023.121390.

References

Affek, H.P., 2013. Clumped isotopic equilibrium and the rate of isotope exchange between CO_2 and water. Am. J. Sci. 313, 309–325.
Affek, H.P., Zaarur, S., 2014. Kinetic isotope effect in CO_2 degassing: insight from clumped and oxygen isotopes in laboratory precipitation experiments. Geochim. Cosmochim. Acta 143, 319–330.
Affek, H.P., Bar-Matthews, M., Ayalon, A., Matthews, A., Eiler, J.M., 2008. Glacial/interglacial temperature variations in Soreq cave speleothems as recorded by "clumped isotope" thermometry. Geochim. Cosmochim. Acta 72, 5351–5360.
Affek, H.P., Matthews, A., Ayalon, A., Bar-Matthews, M., Burstyn, Y., Zaarur, S., Zilberman, T., 2014. Accounting for kinetic isotope effects in Soreq Cave (Israel) speleothems. Geochim. Cosmochim. Acta 143, 303–318.
An, Z., Porter, S.C., Kutzbach, J.E., Xihao, W., Suming, W., Xiaodong, L., Xiaoqiang, L., Weijian, Z., 2000. Asynchronous Holocene optimum of the East Asian monsoon. Quat. Sci. Rev. 19, 743–762.
Asai, K., Tsujimura, M., Fantong, W.Y., 2014. Temporal variation of stable isotope ratios in precipitation on Chubu-mountainous areas: a case study of Mt. Ontake, Japan (in Japanese). J. Jpn. Assoc. Hydrol. Sci. 44, 67–77.
Bintanja, R., van de Wal, R.S.W., 2008. North American ice-sheet dynamics and the onset of 100,000-year glacial cycles. Nature 454, 869–872.
Brand, W.A., Assonov, S.S., Coplen, T.B., 2010. Correction for the ^{17}O interference in $\delta(^{13}C)$ measurements when analyzing CO_2 with stable isotope mass spectrometry (IUPAC Technical Report). Pure Appl. Chem. 82, 1719–1733.
Daëron, M., Guo, W., Eiler, J., Genty, D., Blamart, D., Boch, R., Drysdale, R., Maire, R., Wainer, K., Zanchetta, G., 2011. $^{13}C^{18}O$ clumping in speleothems: Observations from natural caves and precipitation experiments. Geochim. Cosmochim. Acta 75, 3303–3317.
Dansgaard, W., 1964. Stable isotopes in precipitation. Tellus 16, 436–468.
Defliese, W.F., Hren, M.T., Lohmann, K.C., 2015. Compositional and temperature effects of phosphoric acid fractionation on Δ_{47} analysis and implications for discrepant calibrations. Chem. Geol. 396, 51–60.
Dennis, K.J., Affek, H.P., Passey, B.H., Schrag, D.P., Eiler, J.M., 2011. Defining an absolute reference frame for "clumped" isotope studies of CO_2. Geochim. Cosmochim. Acta 75, 7117–7131.
Dorale, J.A., Liu, Z., 2009. Limitations of Hendy Test criteria in judging the paleoclimatic suitability of speleothems and the need for replication. J. Cave Karst Stud. 71, 73–80.
Dreybrodt, W., Fohlmeister, J., 2022. The impact of outgassing of CO_2 and prior calcium precipitation to the isotope composition of calcite precipitated on stalagmites. Implications for reconstructing climate information from proxies. Chem. Geol. 589, 120676.
Eiler, J.M., 2007. "Clumped-isotope" geochemistry—the study of naturally-occurring, multiply-substituted isotopologues. Earth Planet. Sci. Lett. 262, 309–327.
Ford, T.D., Pedley, H.M., 1996. A review of tufa and travertine deposits of the world. Earth Sci. Rev. 41, 117–175.
Fukui, T. (Ed.), 1977. The Climate of Japan. Elsevier, Amsterdam.
Ge, Q., Xue, Z., Yao, Z., Zang, Z., Chu, F., 2017. Anti-phase relationship between the East Asian winter monsoon and summer monsoon during the Holocene? J. Ocean Univ. China 16, 175–183.
Ghosh, P., Adkins, J., Affek, H., Balta, B., Guo, W.F., Schauble, E.A., Schrag, D., Eiler, J. M., 2006. ^{13}C–^{18}O bonds in carbonate minerals: a new kind of paleothermometer. Geochim. Cosmochim. Acta 70, 1439–1456.
Guo, W., 2008. Carbonate Clumped Isotope Thermometry: Application to Carbonaceous Chondrites and Effects of Kinetic Isotope Fractionation. Ph.D. thesis,. Caltech.
Guo, W., Zhou, C., 2019. Patterns and controls of disequilibrium isotope effects in speleothems: Insights from an isotope-enabled diffusion-reaction model and implications for quantitative thermometry. Geochim. Cosmochim. Acta 267, 196–226.
Hanawa, K., Watanabe, T., Iwasaka, N., Suga, T., Toba, Y., 1988. Surface thermal conditions in the Western North Pacific during the ENSO events. J. Meteorol. Soc. Jpn. 66, 445–456.
He, B., Olack, G.A., Colman, A.S., 2012. Pressure baseline correction and high-precision CO_2 clumped-isotope (Δ_{47}) measurements in bellows and micro-volume modes. Rapid Commun. Mass Spectrom. 26, 2837–2853.
Hendy, C.H., 1971. The isotopic geochemistry of speleothems—I: The calculations of the effects of different modes of formation on the isotopic composition of speleothems and their applicability as paleoclimate indicators. Geochem. Cosmochim. Acta 35, 801–824.
Hirose, N., Fukudome, K., 2006. Monitoring the Tsushima warm current improves seasonal prediction of the regional snowfall. SOLA 2, 61–63.
Hori, M., Kawai, T., Matsuoka, J., Kano, A., 2009. Intra-annual perturbations of stable isotopes in tufas: Effects of hydrological processes. Geochim. Cosmochim. Acta 73, 1684–1695.
Hori, M., Ishikawa, T., Nagaishi, K., Lin, K., Wang, B.-S., You, C.-F., Shen, C.-C., Kano, A., 2013. Prior calcite precipitation and source mixing process influence Sr/Ca, Ba/Ca and $^{87}Sr/^{86}Sr$ of a stalagmite developed in southwestern Japan during 18.0 4.5 ka. Chem. Geol. 347, 190–198.
Hori, M., Ishikawa, T., Nagaishi, K., You, C.-F., Huang, K.-F., Shen, C.-C., Kano, A., 2014. Rare earth elements in a stalagmite from southwestern Japan: a potential proxy for chemical weathering. Geochem. J. 48, 73–84.
Kajita, S., Aoyama, S., Kitamura, T., Hibino, M., 1971. The catalogue of limestone caves, Gifu Prefecture, Central Japan 2 (in Japanese). Science report of the Faculty of Education, Gifu University. Nat. Sci. 4, 379–386.
Kano, A., Matsuoka, J., Kojo, T., Fujii, H., 2003. Origin of annual laminations in tufa deposits, Southwest Japan. Palaeogeogr. Palaeoclimatol. Palaeoecol. 191, 243–262.
Kano, A., Okumura, T., Takashima, C., Shiraishi, F., 2019. Geobiochenimal Properties of Travertine with Focus on Japanese Sites. Springer, Singapore.
Kato, H., Yamada, T., 2016. Controlling factors in stalagmite oxygen isotopic composition and the paleoprecipitation record for the last 1,100 years in Northeast Japan. Geochem. J. 50, e1–e6.
Kato, H., Amekawa, S., Kano, A., Mori, T., Kuwahara, Y., Quade, J., 2019. Seasonal temperature changes obtained from carbonate clumped isotopes of annually laminated tufas from Japan: discrepancy between natural and synthetic calcites. Geochim. Cosmochim. Acta 244, 548–564.

Kato, H., Amekawa, S., Hori, M., Shen, C.-C., Kuwahara, Y., Senda, R., Kano, A., 2021. Influences of temperature and the meteoric water $\delta^{18}O$ value on a stalagmite record in the last deglacial to middle Holocene period from southwestern Japan. Quat. Sci. Rev. 253, 106746.
Kawahata, H., Ohshima, H., Kuroyanagi, A., 2011. Terrestrial–Ocean environmental change in the northwestern Pacific from the glacial times to Holocene. J. Asian Earth Sci. 40, 1189–1202.
Kawai, T., Kano, A., Matsuoka, J., Ihara, T., 2006. Seasonal variation in water chemistry and depositional processes in a tufa-bearing stream in SW-Japan, based on 5 years of monthly observations. Chem. Geol. 232, 33–53.
Kigoshi, T., Kumon, F., Hayashi, R., Kuriyama, M., Yamada, K., Takemura, K., 2014. Climate changes for the past 52 ka clarified by total organic carbon concentrations and pollen composition in Lake Biwa, Japan. Quat. Int. 333, 2–12.
Kluge, T., Affek, H.P., 2012. Quantifying kinetic fractionation in Bunker Cave speleothems using Δ_{47}. Quat. Sci. Rev. 49, 82–94.
Kluge, T., Affek, H.P., Marx, T., Aeschbach-Hertig, W., Riechelmann, D.F.C., Scholz, D., Riechelmann, S., Immenhauser, A., Richter, D.K., Fohlmeister, J., Wackerbarth, A., Mangini, A., Spötl, C., 2013. Reconstruction of drip-water $\delta^{18}O$ based on calcite oxygen and clumped isotopes of speleothems from Bunker Cave (Germany). Clim. Past 9, 377–391.
Li, H., Zhang, Q., Yue, P., Zhang, L., Niu, X., Zhang, H., Xing, K., Jing, Y., Shang, G., 2021. Temporal duration of the East Asian summer monsoon substantially affects surface energy exchange over the summer monsoon transition zone of China. J. Clim. 34, 4643–4660.
Lisiecki, L.E., Stern, J.V., 2016. Regional and global benthic δ18O stacks for the last glacial cycle. Paleoceanography 31, 1368–1394.
Liu, X., Dong, H., Yang, X., Herzschuh, U., Zhang, E., Stuut, J.-B.W., Wang, Y., 2009. Late Holocene forcing of the Asian winter and summer monsoon as evidenced by proxy records from the northern Qinghai−Tibetan Plateau. Earth Planet. Sci. Lett. 280, 276–284.
Matthews, A., Affek, H.P., Ayaron, A., Vonhof, H.B., Bar-Matthews, M., 2021. Eastern Mediterranean climate change deduced from the Soreq Cave fluid inclusion stable isotopes and carbonate clumped isotopes record of the last 160 ka. Quat. Sci. Rev. 272, 107223.
Mizota, C., Kusakabe, M., 1994. Spatical distribution of δD-$\delta^{18}O$ values of surface and shallow groundwaters from Japan, South Korea and East China. Geochem. J. 28, 387–410.
Mori, T., Kashiwagi, K., Amekawa, S., Kato, H., Okumura, T., Takashima, C., Wu, C.-C., Shen, C.-C., Quade, J., Kano, A., 2018. Temperature and seawater isotopic controls on two stalagmite records since 83 ka from maritime Japan. Quat. Sci. Rev. 192, 47–58.
Nakagawa, T., Tarasov, P.E., Nishida, K., Gotanda, K., Yasuda, Y., 2002. Quantitative pollen-based climate reconstruction in Central Japan: application to surface and late Quaternary spectra. Quat. Sci. Rev. 21, 2099–2113.
Nakamura, Y., Inouchi, Y., Inoue, T., Kondo, Y., Kumon, F., Nagahashi, Y., 2013. Lake-level changes and their factors during the last 45,000 years in Lake Nojiri, Central Japan (in Japanese). Quatern. Res. (Daiyonki-Kenkyu) 52, 203–212.
NGRIP Members, 2004. High-resolution record of Northern Hemisphere climate extending into the last interglacial period. Nature 431, 147–151.
Porter, S.C., An, Z., 1995. Correlation between climate events in the North Atlantic and China during the last glaciation. Nature 375, 305–308.
Rozanski, K., Araguas-Araguas, L., Gonfiantini, R., 1993. Isotopic patterns in modern global precipitation. Geophys. Monogr. 78, 1–36.
Schauble, E.A., Ghosh, P., Eiler, J.M., 2006. Preferential formation of ^{13}C–^{18}O bonds in carbonate minerals, estimated using first-principles lattice dynamics. Geochim. Cosmochim. Acta 70, 2510–2529.
Scholz, D., Hoffmann, D.L., 2011. StalAge – an algorithm designed for construction of speleothem age models. Quat. Geochronol. 6, 369–382.
Schrag, D.P., Hampt, G., Murray, D.W., 1996. Pore fluid constraints on the temperature and oxygen isotopic composition of the glacial ocean. Sci. 272, 1930–1932.
Schrag, D.P., Adkins, J.F., McIntyre, K., Alexander, J.L., Hodell, D.A., Charles, C.D., McManus, J.F., 2002. The oxygen isotopic composition of seawater during the last Glacial Maximum. Quat. Sci. Rev. 21, 331–342.
Shakun, J.D., Lea, D.W., Lisiecki, L.E., Raymo, M.E., 2015. An 800-kyr record of global surface ocean $\delta^{18}O$ and implications for ice volume-temperature coupling. Earth Planet. Sci. Lett. 426, 58–68.
Shen, C.-C., Kano, A., Hori, M., Lin, K., Chiu, T.-C., Burr, G.S., 2010. East Asian monsoon evolution and reconciliation of climate records from Japan and Greenland during the last deglaciation. Quat. Sci. Rev. 29, 3327–3335.
Song, J.-L., Sun, H.-Y., Tian, M.-Z., Zhang, X.-J., Wen, X.-F., Sun, M., 2018. Heinrich events recorded in a loessepaleosol sequence from Hexigten, Inner Mongolia. Geosci. Front. 9, 431–439.
Steinke, S., Glatz, C., Mohtadi, M., Groeneveld, J., Li, Q., Jian, Z., 2011. Past dynamics of the East Asian monsoon: no inverse behaviour between the summer and winter monsoon during the Holocene. Glob. Planet. Chang. 78, 170–177.
Tanoue, M., Ichiyanagi, K., Shimada, J., 2013. Seasonal variation and spatial distribution of stable isotopes in precipitation over Japan (in Japanese). J. Jpn. Assoc. Hydrol. Sci. 43, 73–91.
Tremaine, D.M., Froelich, P.N., Wang, Y., 2011. Speleothem calcite farmed in situ: Modern calibration of $\delta^{18}O$ and $\delta^{13}C$ paleoclimate proxies in a continuously-monitored natural cave system. Geochim. Cosmochim. Acta 75, 4929–4950.
Uemura, R., Nakamoto, M., Asami, R., Mishima, S., Gibo, M., Msaka, K., Chen, J.-P., Wu, C.-C., Chang, Y.-W., Shen, C.-C., 2016. Precise oxygen and hydrogen isotope determination in nanoliter quantities of speleothem inclusion water by cavity ring-down spectroscopic techniques. Geochim. Cosmochim. Acta 172, 159–176.
Wainer, K., Genty, D., Blamart, D., Daëron, M., Bar-Matthews, M., Vonhof, H., Dublyansky, Y., Pons-Branchu, E., Thomas, L., van Calsteren, P., Quinif, Y., Caillon, N., 2011. Speleothem record of the last 180 ka in Villars cave (SW France): investigation of a large $\delta^{18}O$ shift between MIS6 and MIS5. Quat. Sci. Rev. 30, 130–146.
Wang, Y.J., Cheng, H., Edwards, R.L., An, Z.S., Wu, J.Y., Shen, C.-C., Dorale, J.A., 2001. A high-resolution absolute-dated late pleistocene monsoon record from Hulu Cave, China. Science 451, 1090–1093.
Wanner, H., Beer, J., Bütikofer, J., Crowley, T.J., Cubasch, U., Flückiger, J., Goosse, H., Grosjean, M., Joos, F., Kaplan, J.O., Küttel, M., Müller, S.A., Prentice, I.C., Solomina, O., Stocker, T.F., Tarasov, P., Wagner, M., Widmann, M., 2008. Mid- to late Holocene climate change: an overview. Quat. Sci. Rev. 27, 1791–1828.
Wassenburg, J.A., Vonhof, H.B., Cheng, H., Martínez-García, A., Ebner, P.-R., Li, X., Zhang, H., Sha, L., Tian, Y., Edwards, R.L., Fiebig, J., Haug, G.H., 2021. Penultimate deglaciation Asian monsoon response to North Atlantic circulation collapse. Nat. Geosci. 14, 937–941.
Xiao, J., Porter, S.C., An, Z., Kumai, H., Yoshikawa, S., 1995. Grain size of quartz as an indicator of winter monsoon strength on the Loess Plateau of Central China during the last 130,000 yr. Quat. Res. 43, 22–29.
Yan, M., Liu, Z.Y., Ning, L., Liu, J., 2020. Holocene EASM-EAWM relationship across different timescales in CCSM3. Geophys. Res. Lett. 47, e2020GL088451.
Yancheva, G., Nowaczyk, N.R., Mingram, J., Dulski, P., Schettler, G., Negendank, J.F.W., Liu, J., Sigman, D.M., Peterson, L.C., Haug, G.H., 2007. Influence of the intertropical convergence zone on the East Asian monsoon. Nature 445, 74–77.
Yura, K., 2011. Visit and consideration of Ohtaki Limestone Cave (tourism cave), Gujo City, Gifu Prefecture (in Japanese). Cave Environ. NET Soci. 2, 3–10.
Zhang, D., Lu, L., 2007. Anti-correlation of summer/winter monsoons? Nature 450, E7–E8.